

Titania nanosheets induce anticancer activity
in human non-small cell lung cancer cells



A Dissertation Submitted in Partial Fulfillment of the Requirements
for the Degree of Doctor of Philosophy in Pharmacology
Inter-Department of Pharmacology
GRADUATE SCHOOL
Chulalongkorn University
Academic Year 2022
Copyright of Chulalongkorn University

สารโศกนาฏกรรมโน้ตที่เหนียวนำไปเกิดฤทธิ์การต้านมะเร็งต่อเซลล์มะเร็งปอด
ชนิดไม่ใช่เซลล์เล็กของมนุษย์



วิทยานิพนธ์นี้เป็นส่วนหนึ่งของการศึกษาตามหลักสูตรปริญญาวิทยาศาสตรดุษฎีบัณฑิต
สาขาวิชาเภสัชวิทยา (สหสาขาวิชา) สหสาขาวิชาเภสัชวิทยา
บัณฑิตวิทยาลัย จุฬาลงกรณ์มหาวิทยาลัย
ปีการศึกษา 2565
ลิขสิทธิ์ของจุฬาลงกรณ์มหาวิทยาลัย

Thesis Title	Titania nanosheets induce anticancer activity in human non-small cell lung cancer cells
By	Miss Rapeepun Soonnarong
Field of Study	Pharmacology
Thesis Advisor	Professor PITHI CHANVORACHOTE, Ph.D.

Accepted by the GRADUATE SCHOOL, Chulalongkorn University in Partial Fulfillment of the Requirement for the Doctor of Philosophy

..... Dean of the GRADUATE SCHOOL
(Associate Professor YOOTTHANA CHUPPUNNARAT, Ph.D.)

DISSERTATION COMMITTEE

..... Chairman
(Associate Professor SUREE JIANMONGKOL, Ph.D.)

..... Thesis Advisor
(Professor PITHI CHANVORACHOTE, Ph.D.)

..... Examiner
(Associate Professor PIYANUCH WONGANAN, Ph.D.)

..... Examiner
(Associate Professor SIREERAT SOOAMPON, Ph.D.)

..... External Examiner
(Associate Professor Uraiwan Panich, Ph.D.)

รพีพรรณ สุณรรงค์ : สารไททาเนียนาโนซีทเหนี่ยวนำให้เกิดฤทธิ์การต้านมะเร็งต่อ เซลล์มะเร็งปอดชนิดไม่ใช่เซลล์เล็กของมนุษย์. (Titania nanosheets induce anticancer activity in human non-small cell lung cancer cells) อ.ที่ปรึกษาหลัก : ศ. ดร.ปิติ จันทรวรโชติ

โลหะอนุภาคนาโนถูกนำไปใช้ประโยชน์ในการรักษามะเร็ง ในที่นี้เราแสดงให้เห็นถึงสารไททาเนียนาโนซีททำให้เกิดความเป็นพิษต่อเซลล์มะเร็งปอดหลายๆ ชนิดแต่ไม่เกิดขึ้นกับเซลล์ปกติ เซลล์มะเร็งปอดที่ได้รับสารไททาเนียนาโนซีทจะแสดงให้เห็นลักษณะการตายแบบอะพอพโทซิส การวิเคราะห์โปรตีนยังระบุเพิ่มเติมถึงการกระตุ้นกลไกการตายที่ขึ้นอยู่กับ p53 กล้องจุลทรรศน์อิเล็กตรอนแบบส่องผ่าน (TEM) และ กล้องจุลทรรศน์อิเล็กตรอนแบบส่องกราด (SEM) แสดงให้เห็นการเข้าเซลล์ของนาโนซีทและชักนำให้เซลล์เกิดการเปลี่ยนแปลงรูปร่าง ไททาเนียนาโนซีททำให้เซลล์เกิดการตายแบบอะพอพโทซิสผ่านกลไกการสร้างเปอร์ออกซีไนไตรท์ (ONOO⁻) เป็นที่ทราบอยู่แล้วว่าเปอร์ออกซีไนไตรท์เป็นตัวที่มีศักยภาพในการเหนี่ยวนำให้เกิดเอส-ไนโตรซิเลชัน (S-nitrosylation) ซึ่งพบว่านาโนซีทเป็นสื่อกลางทำให้เกิดเอส-ไนโตรซิเลชันของ p53 ที่ตำแหน่ง C182 เป็นผลให้เพิ่มเสถียรภาพของโปรตีน-โปรตีนคอมเพล็กซ์มากขึ้นและมีแนวโน้มจะชักนำตำแหน่งโดยรอบจับกันแน่นมากยิ่งขึ้น วิเคราะห์พลวัตโมเลกุลแสดงให้เห็นเพิ่มเติมว่าการเกิดเอส-ไนโตรซิเลชันที่ตำแหน่ง C182 ทำให้โมเลกุลคู่ของ p53 เสถียรโดยแสดงให้เห็นพลังงานอิสระกิบส์ < -1.5 kcal/mol ด้วยผลลัพธ์เหล่านี้ให้ข้อมูลเชิงลึกใหม่ต่อการเหนี่ยวนำให้เกิดการตายแบบอะพอพโทซิสที่ส่งผลมาจากนาโนซีทผ่านกลไกระดับโมเลกุลเกิดเอส-ไนโตรซิเลชันของโปรตีน p53 โดยเน้นถึงกลไกในการออกฤทธิ์ของวัสดุนาโนเพื่อการรักษามะเร็ง

สาขาวิชา เกษษัตริศาสตร์ (สหสาขาวิชา)

ปีการศึกษา 2565

ลายมือชื่อนิสิต

ลายมือชื่อ อ.ที่ปรึกษาหลัก

5987819320 : MAJOR PHARMACOLOGY

KEYWORD: apoptosis, nanosheets, lung cancer, p53, S-nitrosylation,
peroxynitrite, molecular dynamics

Rapeepun Soonnarong : Titania nanosheets induce anticancer activity in human non-small cell lung cancer cells. Advisor: Prof. PITHI CHANVORACHOTE, Ph.D.

Metal nanomaterials can enhance the efficacy of current cancer therapies. Here, we show that $Ti_{0.8}O_2$ nanosheets cause cytotoxicity in several lung cancer cells but not in normal cells. The nanosheet-treated cells showed certain apoptosis characteristics. Protein analysis further indicated the activation of the p53-dependent death mechanism. Transmission electron microscopy (TEM) and scanning electron microscopy (SEM) analyses revealed the cellular uptake of the nanosheets and the induction of cell morphological change. $Ti_{0.8}O_2$ nanosheets induce apoptosis through a molecular mechanism involving peroxynitrite ($ONOO^-$) generation. As peroxynitrite is known to be a potent inducer of S-nitrosylation, we further found that the nanosheets mediated the S-nitrosylation of p53 at C182, resulting in higher protein-protein complex stability, and this was likely to induce the surrounding residues, located in the interface region, to bind more strongly to each other. Molecular dynamics analysis revealed that S-nitrosylation stabilized the p53 dimer with the binding free energy of <-1.5 kcal/mol. These results provide novel insight on the apoptosis induction effect of the nanosheets via a molecular mechanism involving S-nitrosylation of the p53 protein, emphasizing the mechanism of action of nanomaterials for cancer therapy.

Field of Study: Pharmacology

Student's Signature

Academic Year: 2022

Advisor's Signature

ACKNOWLEDGEMENTS

First and foremost, I would like to express my sincere thanks to my thesis advisor, Professor Pithi Chanvorachote (Ph.D.) for his invaluable help and constant encouragement throughout the course of this research. I am most grateful for his teaching and advice, not only the research methodologies but also many other methodologies in life. I would not have achieved this far and this thesis would not have been completed without all the support that I have always received from him.

In addition, I am grateful for the teachers of Interdisciplinarity Pharmacology, Chulalongkorn University and others person for suggestions and all their help.

My special thanks are extended to all co-authors in my publications for their kindly helps, advices, and abundant encouragements throughout the research. Their creativity will continue to inspire me forever.

I appreciate to thank grants as follows: “The Thailand Research Fund through the Royal Golden Jubilee Ph.D. program (Grant No. PHD/0135/2559).” which supported my researches and my life while I was Ph.D. student.

Moreover, I would like to thank all my colleagues at Faculty of Pharmaceutical Sciences and Department of Pharmacology, Chulalongkorn University for their friendships and supports.

Finally, I would like to express my appreciation to my dearest parents for their love, kindness, and meaningful supports through my life. Thanks to Dr. Sucharat Tungskruthai for their friendship in the lab. You supported me greatly and were always willing to help me, as well as Ratchapol Soonnarong for their gives encouragement while I was Ph.D. student.

Rapeepun Soonnarong

TABLE OF CONTENTS

	Page
ABSTRACT (THAI).....	iii
ABSTRACT (ENGLISH).....	iv
ACKNOWLEDGEMENTS	v
TABLE OF CONTENTS	vi
LIST OF FIGURES	ix
Objectives.....	15
Hypothesis.....	15
Conceptual framework.....	16
Research design	17
Expected benefits and applications	1
LITERATURE REVIEWS.....	2
Lung cancer.....	2
Apoptosis.....	10
Role of p53 in apoptosis	13
Structural stability of the p53 tetramer	15
Role of reactive oxygen species (ROS) in apoptosis induction.....	17
Nitric oxide (NO) induce apoptosis.....	19
Crosstalk between ROS and NO in control of p53	21
Ti _{0.8} O ₂ nanosheets.....	23
Cancer treatment approaches based on nanomaterials.....	27
MATERIALS AND METHODS	29

Chemicals	29
Test compound.....	30
Cell culture	31
Patient-derived primary lung cancer cell line preparation from malignant pleural effusion	31
Methodes.....	32
1. Cytotoxicity assay.....	32
2. Nuclear staining assay	32
3. Cell apoptosis analysis.....	33
4. Scanning Electron Microscopy (SEM) morphological analysis.....	33
5. Transmission Electron Microscopy (TEM) for cellular uptake analysis.....	34
6. Western Blot analysis	34
7. ROS, superoxide anion, and hydroxyl radical detection by flow cytometry. 34	
8. NO detection by DAF-FM DA assay	35
9. Immunofluorescence	35
10. Cycloheximide (CHX) chasing assay	36
11. Immunoprecipitation assay.....	36
12. S-Nitrosylated protein detection	36
13. Computational method.....	37
Statistical analysis	38
RESULTS.....	39
1. Cytotoxicity of the $Ti_{0.8}O_2$ nanosheets on human lung cancer cells and normal cells	39
2. Effect of $Ti_{0.8}O_2$ nanosheets on apoptosis in human lung cancer cells.....	40

3. Uptake of the $Ti_{0.8}O_2$ nanosheets by cancer cells.....	42
4. $Ti_{0.8}O_2$ nanosheets modulate apoptosis-related proteins in H460 and A549 cells	44
5. Cytotoxicity and apoptotic effects of $Ti_{0.8}O_2$ nanosheets on advanced lung cancer cells from patients	45
6. Effect of $Ti_{0.8}O_2$ Nanosheets on intracellular ROS induction in A549 and H460 cells	48
7. $Ti_{0.8}O_2$ nanosheet-mediated peroxynitrite induces apoptosis in A549 and H460 cells	52
Figure 23 $Ti_{0.8}O_2$ nanosheet-mediated peroxynitrite induces apoptosis in A549 and H460 cells.....	55
8. $Ti_{0.8}O_2$ nanosheet-mediated peroxynitrite induces apoptosis in lung cancer cells via p53 upregulation	55
9. $Ti_{0.8}O_2$ nanosheets increase p53 function but not through p53 proteasomal degradation	57
10. S-nitrosylation in the regulation of stability of the tetrameric p53 protein- protein complex	60
DISCUSSION.....	66
CONCLUSIONS	75
REFERENCES	76
VITA.....	95

LIST OF FIGURES

	Page
Figure 1 Stages of lung cancer (29).....	7
Figure 2 Extrinsic and intrinsic apoptotic signaling pathways (35).....	11
Figure 3 Mechanisms of p53-induced apoptosis (40).....	15
Figure 4 The 3D structure model of p53 tetramer (47).....	16
Figure 5 Activation of the mitochondrial (intrinsic) pathway of apoptosis by ROS (53)	19
Figure 6 NO production and targets of NO-mediated signaling (56).....	21
Figure 7 Schematic diagram describing the mechanisms implicated in NP-induced ROS production (69).....	24
Figure 8 Effect of Ti _{0.8} O ₂ nanosheets on cell viability of lung cancer cells.....	39
Figure 9 Effect of Ti _{0.8} O ₂ nanosheets on cell viability of normal cells.....	40
Figure 10 Effect of Ti _{0.8} O ₂ nanosheets on characteristic apoptosis cells by a nuclear staining assay.....	41
Figure 11 Effect of Ti _{0.8} O ₂ nanosheets on characteristic apoptosis cells by annexin V- FITC/PI staining with flow cytometry.....	42
Figure 12 Morphology of H460 cells determined by scanning electron microscopy (SEM).....	43
Figure 13 Cellular uptake of Ti _{0.8} O ₂ nanosheets in H460 and primary DP cells at 24 h by transmission electron microscopy (TEM).....	43
Figure 14 Effect of Ti _{0.8} O ₂ nanosheets on apoptosis-related proteins.....	45
Figure 15 Cytotoxicity of the Ti _{0.8} O ₂ nanosheets on malignant pleural effusion from advanced lung cancer patients.....	46

Figure 16 Effect of $Ti_{0.8}O_2$ nanosheets, Cisplatin and Etoposide on characteristic apoptosis cells by a nuclear staining assay of malignant pleural effusion from advanced lung cancer patients	47
Figure 17 The effect of $Ti_{0.8}O_2$ nanosheets on intracellular ROS induction	49
Figure 18 Effect of $Ti_{0.8}O_2$ nanosheets on cell viability with the pretreatment of ROS scavenger.....	50
Figure 19 Effect of $Ti_{0.8}O_2$ nanosheets on intracellular superoxide anions induction..	51
Figure 20 Effect of $Ti_{0.8}O_2$ nanosheets on intracellular hydroxyl radicals induction	52
Figure 21 $Ti_{0.8}O_2$ nanosheets induced NO in A549 and H460 cells and mediated peroxynitrite generation	53
Figure 22 Cellular NO level stained with DAF-FM DA in cells treated with $Ti_{0.8}O_2$ nanosheets.....	54
Figure 23 $Ti_{0.8}O_2$ nanosheet-mediated peroxynitrite induces apoptosis in A549 and H460 cells.....	55
Figure 24 Peroxynitrite-potentiated cell apoptosis through the p53 protein	56
Figure 25 The expressions of p53 and P-p53 were analyzed by immunofluorescence staining in A549 and H460 cells.....	57
Figure 26 Effect of $Ti_{0.8}O_2$ nanosheets on the half-life of p53	58
Figure 27 The half-lives of the p53 protein in the $Ti_{0.8}O_2$ nanosheet-treated cells	59
Figure 28 $Ti_{0.8}O_2$ nanosheet decreases ubiquitin-mediated p53 proteasomal degradation	60
Figure 29 Three-dimensional (3D) structure of the tetrameric p53	61
Figure 30 Time evolution of the total number of intermolecular hydrogen bonds formed between each monomer of the p53 core domain and its adjacent monomer	62

Figure 31 The total contributing energy from each amino acid of the tetrameric p53 protein–protein complex.....	63
Figure 32 The representative 3D structure taken from the last MD snapshot of the S-nitrosylation system.....	64
Figure 33 $Ti_{0.8}O_2$ induction of S-nitrosylation in the cells.....	65
Figure 34 Schematic diagram of $Ti_{0.8}O_2$ nanosheet-mediated peroxynitrite generation that was associated with apoptosis via p53 upregulation in non-small cell lung cancer	74



Background and rationale

Lung cancer is one of the most common cancers and accounts the highest mortality rate. Although crucial components of the fight against lung cancer including the small molecule tyrosine kinase inhibitors and immunotherapy have led to unprecedented survival benefits in selected patients, the overall cure and survival rates for non-small cell lung cancer (NSCLC) remain low (1). Therefore, continued research into new drugs and combination therapies is required to expand the clinical benefit to a broader patient population and to improve outcomes in NSCLC. The tumor suppressor p53 is an essential regulatory molecule that is implicated in cell cycle arrest and plays a mediator of apoptosis in response to stress (2). A key attribute of the p53 response is p53 stabilization, as a result rapid increase in p53 steady-state levels. Considerable evidence indicates that p53 stabilization largely depends on post-translational events that disengage p53 from its proteasomal degradation (3). At all cases of this includes a series of post-translational modifications, some of which are known to impact the interaction between p53 and MDM2, that the major mechanism for controlling p53 stability (4). The activation of p53 results in the increase of BH3-only proteins promoted BAX/BAK oligomerization. The induction of pro-apoptotic signaling leads to the formation of mitochondrial pores, the release of cytochrome c into the cytosol, the activation of caspases and finally cell apoptosis (5). In contrast, dysregulation of apoptosis in lung cancer can be caused by several mechanisms;

however, the up-regulation of expression of pro-survival proteins including mammalian target of rapamycin (mTOR), and anti-apoptotic proteins of the Bcl-2 family were shown to be the predominant mechanisms (6).

The p53, an important tumor suppressor protein, has been intensively investigated as its functions are critical for cancers. The function of p53 protein tightly associates with its protein conformation. Active conformation of this protein is the tetrameric form via an interaction of tetramerization domain (TD) on p53 protein. Studies have pointed out that the tetramerization of p53 is critical for DNA binding, post-translational modifications, as well as p53 stability (7). Cysteine thiol groups on the p53 molecule were pointed to be the sensitive sites for protein modification and DNA binding affinity was shown to be altered by thiol blocking agents (8). Certain cysteine residue amino acid replacements inhibit binding of p53 to DNA (9). In addition, several lines of evidence have demonstrated that oxidative modification of cysteine residues within p53 can also influence the protein's activity and stability (10-12).

Nitric oxide (NO) is a key intercellular messenger synthesized from L-arginine in a reaction catalyzed by NO synthases (NOS). Nitric oxide has appeared as an important signaling device for controlling practically all critical cellular function, also a strong mediator of cellular damage (13-15). Nitric oxide plays an extensive role in regulating the expression of eukaryotic genes, and this effect is exerted in part through S-nitrosylation (14). S-Nitrosylation of controlling binding associates of

transcription factors can exert an extranuclear effect on transcription factor activation, stability, and/or nuclear targeting, as in the case of hypoxia-inducible factor-1 α (HIF-1 α) and p53 (16). In addition, nitric oxide can be reacted with superoxide ($O_2^{\cdot-}$) to form the much more powerful oxidant peroxynitrite ($ONOO^-$) which is a key component to determine the contrasting roles of nitric oxide in physiology and pathology (17). Many of the biological effects ascribe to nitric oxide are factually intermediate by peroxynitrite. Even though peroxynitrite is a powerful oxidant, it reacts at a moderately slow rate with most biological molecules and is competent to reach cell membranes in part through anion channels (18). That makes the biological and pathological insinuations of peroxynitrite much more arresting because it can have more delicate and specific actions on cells.

Nanotechnology is a research field which has implications in the fields of chemistry, engineering, biology, and medicine. Nanotechnology has several applications in cancer biology, especially the development of novel treatments (19). Nanosheets are a developing class of nanomaterial which is highly anisotropic and flexible (20). Moreover, $Ti_{0.8}O_2$ nanosheets also induced superoxide anion in cancer without harming normal dermal papilla cells (21). However, the nanotoxicity and mechanism of $Ti_{0.8}O_2$ nanosheets for specific site-targeting strategies in NSCLC have not been investigated. Therefore, this study aims to investigate the effects of $Ti_{0.8}O_2$ nanosheets on the cytotoxicity of human non-

small cell lung cancer (NSCLC) cells and identify the molecular mechanisms of toxicity of these cells, which is related to ROS generation-mediated apoptosis via the mitochondrial pathway. This study could be valuable in the development of nanomaterials for anti-cancer approaches.

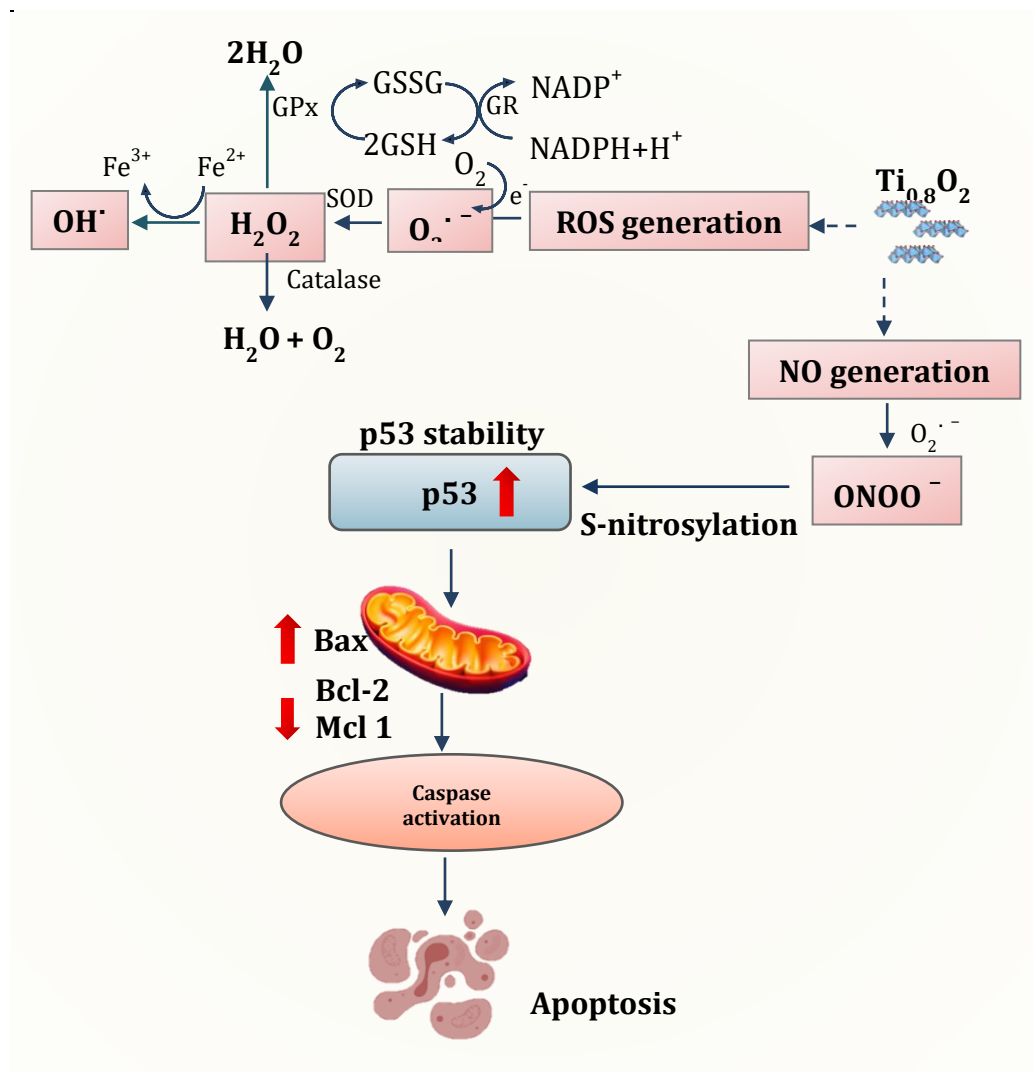
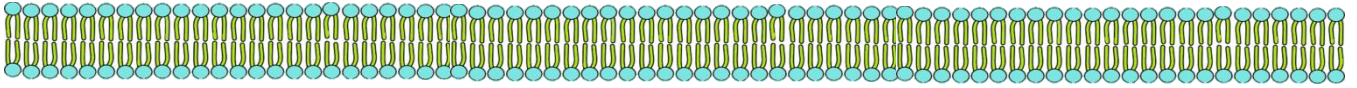
Objectives

1. To investigate the effects of $Ti_{0.8}O_2$ nanosheets on lung cancer cells.
2. To elucidate the underlying mechanisms of these effects caused by $Ti_{0.8}O_2$ nanosheets on lung cancer cells.

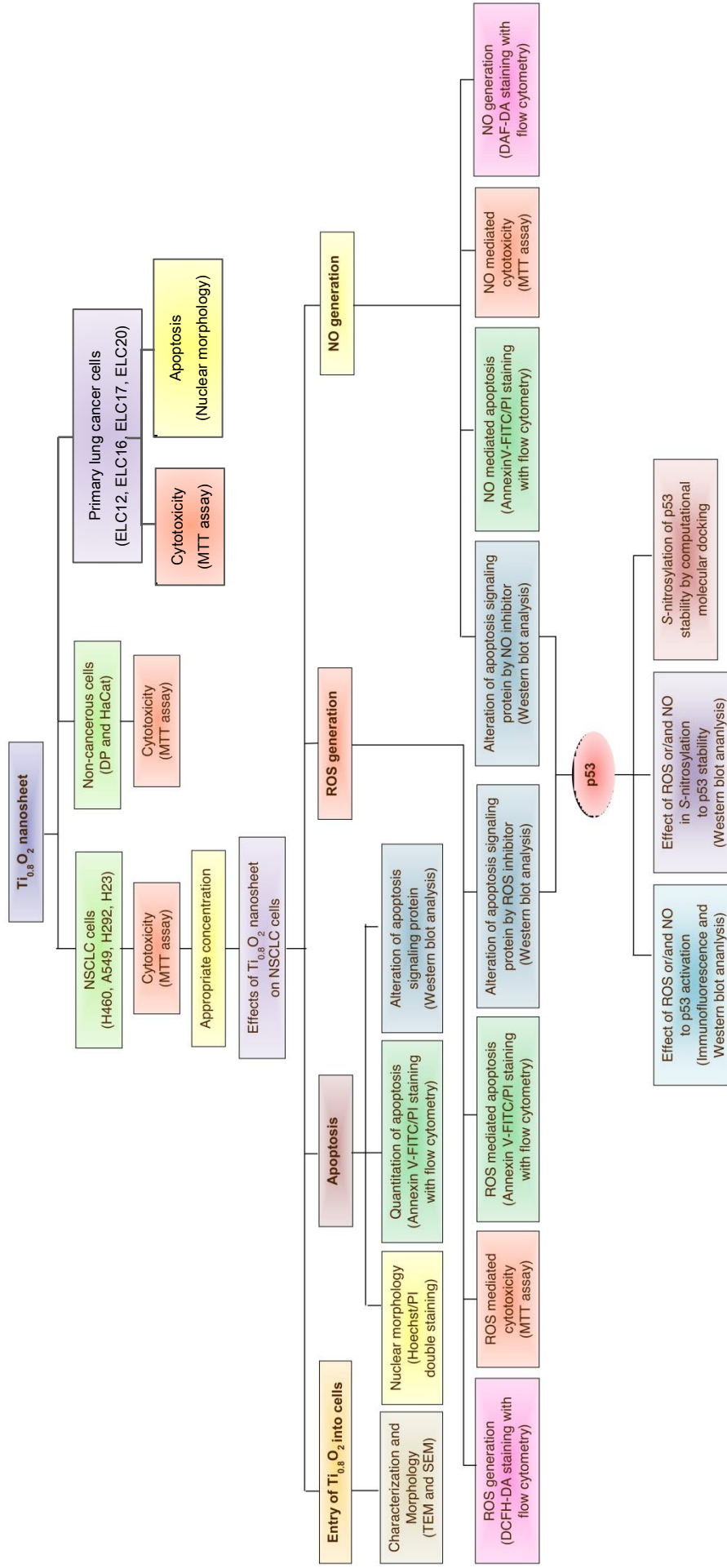
Hypothesis

$Ti_{0.8}O_2$ nanosheets induces apoptosis induction in NSCLC cells through a molecular mechanism involving peroxynitrite generation, it may directly control p53 by S-nitrosylation to stabilize the tetrameric structure of this protein.

Conceptual framework



Research design



Expected benefits and applications

The results of this study will provide the mechanism of $Ti_{0.8}O_2$ nanosheets to induce apoptosis in non-small cells lung cancer. This information will provide a benefit for further development of $Ti_{0.8}O_2$ nanosheets to gain more efficacy and p53 stability targeting activity or approach for research and development of anti-cancer drug.



LITERATURE REVIEWS

Lung cancer

Lung cancer is raised from normal epithelial cells of the airway and alveolar which continuously genetic damage leading to an uncontrolled proliferation and abnormal cells growth in the lung. Lung cancer is the most commonly occurring cancer in the world. In terms of mortality rate, lung cancer is the first (1.8 million death cases, 18.4% of total cases) most common cause of estimated cancer death in 2020 (2.21 million cases) (22). Interestingly, the primarily causes of cancer-related death are dependent on their chemotherapeutic resistance and recurrence capabilities. In Thailand, lung cancer is noted to be the most common type of cancer in Thailand and accounted for 14.1% of all types of cancers (of which, 70% were diagnosed in the advanced disease stage). In addition, lung cancer has the second-highest mortality rate (18.7%) in Thailand next to liver cancer, which has the highest mortality rate (20.3%) as of 2018 (23).

In general, lung cancer can be divided into two major types by histology, non-small cell lung cancer (NSCLC; about 85% of all lung cancers) and small-cell lung cancer (SCLC; about 15%) (24). Smoking is the most important risk factor for all types of lung cancer; 80% of lung cancer cases are the results of smoking (25). NSCLC has four main stages. In the limited stage, cancer is found in only one lung or nearby lymph nodes on the same side of the chest, whereas the extensive stage means that

cancer has spread to both lungs, into the area around the lungs, or to distant organs (26).

At the present day, surgery, radiation, chemotherapy, targeted therapy, and immunotherapy are used in lung cancer treatment. However, there are still problematic aspects of this treatment, for example some cancer patients displaying drug resistance and significant side effects when treated with cisplatin (first-line drug for NSCLC) (24). Therefore, this is the reason why new therapeutic strategies are required for lung cancer treatment. From the fact that several chemotherapeutic and targeted therapeutic drugs use programmed cell death; apoptosis as the main mechanism to treat cancer, apoptotic cell death is further mentioned (27).

Stages of lung cancer

Lung cancer is a disease that develops in lung tissues, especially in the lining of the airways. Non-small cell lung cancer (NSCLC) and small cell lung cancer (SCLC) are the two most common types. NSCLC is the more common of the two, accounting for 80-85 % of all lung cancers, according to the American Cancer Society (ACS). The IASLC staging committee defined stage groupings in the following as figure 1. However, the definition of the stage groups has frequently classified the stages of NSCLC and SCLC using the TNM system, which stands for:

- T-the size of the main tumor: Has it spread to other organs or tissues nearby?
- N-nodes: Has the cancer metastasized to nearby lymph nodes?

- M-metastasis: Has the cancer metastasized to distant organs, such as the brain, bones, the other lung, or other areas?

NSCLC cancer is categorized by the following five stages, depending on when it's discovered:

Stage 0

Detect abnormal cells in the lining of your air passages. These may turn cancerous and affect normal tissue nearby, but they have not spread throughout other parts of the body.

The subtypes of stage 0 NSCLC are:

- Adenocarcinoma in situ—when abnormal cells are detected in glandular tissue lining the lungs.
- Squamous cell carcinoma in situ—when abnormal cells are detected in the tissues that line the respiratory tract. These cells may turn cancerous and affect other nearby tissues.

Stage I

In this stage, abnormal cells have turned into cancer.

- Stage IA: The cancer affects the lung only, with a tumor that measures 3 cm or smaller and has not spread to lymph nodes or other areas.
- Stage IB: In some cases, the lung cancer tumor is larger than 3 cm, but smaller than 4 cm, and has not metastasized to lymph nodes.

In other cases, the lung cancer tumor measures 4 cm or smaller and meets at least one of the following criteria:

- The cancer has reached the main bronchus (a large airway connecting the trachea to the lung), but not the carina (a ridge at the bottom of the trachea that divides the openings of the left and right main bronchi).
- The cancer has reached the innermost tissue that wraps around the lung.
- Either a portion of or the entire lung has collapsed or has pneumonitis (a condition in which the lung becomes inflamed).
- The cancer has not reached nearby lymph nodes.

Stage II

Stage II cases are further classified into two subtypes:

- Stage IIA: The lung cancer tumor is smaller than 5 cm, but larger than 4 cm, and has not metastasized to the lymph nodes.
- Stage IIB: The lung cancer tumor measures 5 cm or smaller and has reached lymph nodes located in the same area of the chest as the original tumor—typically lymph nodes in the lung or close to the bronchus.

Stage III

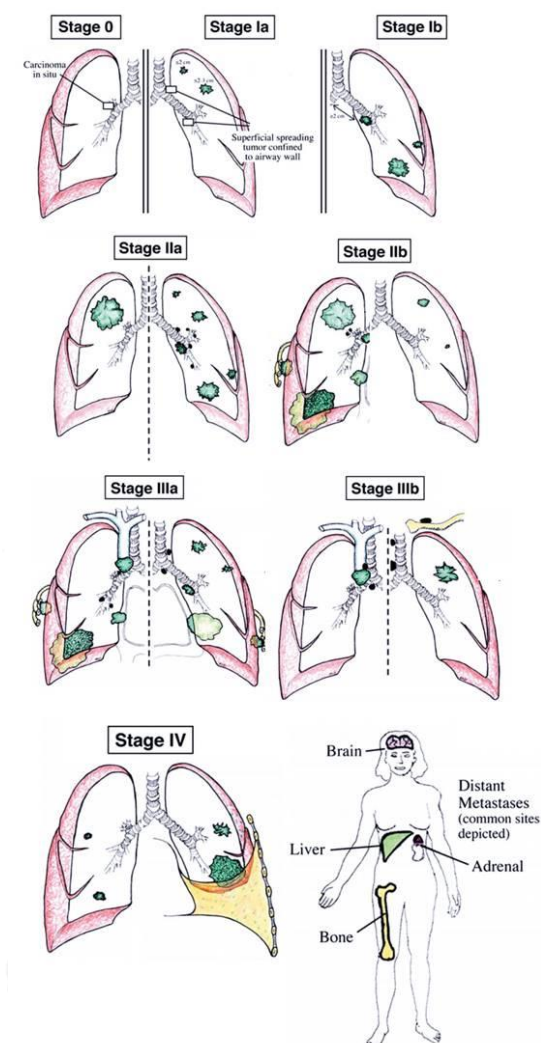
Cases of stage III NSCLC are classified into two subtypes:

- Stage IIIA: The lung cancer tumor measures 5 cm or smaller and has reached lymph nodes in the same area of the chest where the original tumor was detected—typically, the lymph nodes in the trachea, aorta of the heart or where the trachea splits into bronchi.
- Stage IIIB: The lung cancer tumor is 5 cm or smaller, and the cancer has reached the lymph nodes above the collarbone in the same area of the chest as the original tumor, or lymph nodes on the other side of the chest.

Stage IV

Cases of stage IV NSCLC are classified by the lung cancer tumor is any size, may have reached the lymph nodes, and meets at least one of the following criteria:

- At least one tumor has formed in the lung opposite to where the original tumor formed.
- The cancer has reached the sac around the heart or the tissues wrapping around the lungs.
- The cancer has spread to fluid surrounding the heart or lungs.
- The cancer has reached an organ far away from the lung, such as the brain, liver or kidney.
- The cancer has reached various places in at least one organ far away from the lung (28)



จุฬาลงกรณ์มหาวิทยาลัย
Figure 1 Stages of lung cancer (29)
CHULALONGKORN UNIVERSITY

Treatment for lung cancer

Many technical, pharmacological and service developments have been made in the staging and treatment of lung cancer over the past 10 years, but questions still remain about how to best implement these and their cost effectiveness. Further research is needed to ascertain whether newer radiotherapy techniques, such as SABR are equivalent to surgery for early state

age lung cancers (30). Much discussion still surrounds the newer targeted agents' cost effectiveness and whether improving early supportive care might be a good use of resources. In this section, the standard and treatment options for lung cancer can include (24, 31, 32):

- **Surgery:** Surgery to remove the cancer might be an option for early-stage NSCLC. It provides the best chance to cure the disease. But lung cancer surgery is a complex operation that can have serious consequences, so it should be done by a surgeon who has a lot of experience operating on lung cancers.
- **Radiation therapy:** Radiation therapy uses high-powered energy beams from sources such as X-rays and protons to kill cancer cells. Radiation may be used before surgery or after surgery. It's often combined with chemotherapy treatments. For advanced lung cancers and those that have spread to other areas of the body, radiation therapy may help relieve symptoms, such as pain.
- **Chemotherapy:** Chemotherapy uses drugs to kill cancer cells. Chemotherapy is often used after surgery to kill any cancer cells that may remain. It can be used alone or combined with radiation therapy. The chemo drugs most often used for NSCLC such as Cisplatin, Carboplatin, Paclitaxel etc.

- Stereotactic body radiotherapy (SABR): Also known as radiosurgery, is an intense radiation treatment that aims many beams of radiation from many angles at the cancer. SABR may be an option for people with small lung cancers who can't undergo surgery. It may also be used
- Targeted drug therapy: Treatments focus on specific abnormalities present within cancer cells. By blocking these abnormalities, targeted drug treatments can cause cancer cells to die -
 - Drugs that target tumor blood vessel growth (angiogenesis): Bevacizumab
 - Drugs that target cells with *KRAS* gene changes: Sotorasib
 - Drugs that target cells with *EGFR* gene changes: Erlotinib
 - Drugs that target cells with *ALK* gene changes: Crizotinib
 - Drugs that target cells with *ROS1* gene changes: Lorlatinib
 - Drugs that target cells with *BRAF* gene changes: Dabrafenib
 - Drugs that target cells with *RET* gene changes: Selpercatinib
 - Drugs that target cells with *MET* gene changes: Capmatinib
 - Drugs that target cells with *NTRK* gene changes: Larotrectinib
- Immunotherapy: Treatment uses your immune system to fight cancer. Your body's disease-fighting immune system may not attack your cancer because the cancer cells produce proteins that help them

hide from the immune system cells. Immunotherapy works by interfering with that process.

- Palliative care: People with lung cancer often experience signs and symptoms of the cancer, as well as side effects of treatment. Supportive care, also known as palliative care, is a specialty area of medicine that involves working with a doctor to minimize your signs and symptoms. Those receiving supportive care reported improved mood and quality of life. They survived, on average, almost three months longer than did those receiving standard care.

Apoptosis

Apoptosis play an important role during lung cancer progression. Apoptosis is regulated by intracellular and/or extracellular signals and characterized by morphological changes of the cell targeted for death that include nuclear fragmentation and condensation, mitochondrial outer membrane permeabilization (MOMP), membrane blebbing, cell shrinkage and apoptotic body formation (33). In order to survive, cancer cells must develop the highly efficient, and usually multiple mechanisms to avoid apoptosis. Apoptosis is regulated by activation of proteins in caspase family which are central to the mechanism of apoptosis (34). The two

signaling pathways for an initiation of apoptosis are known as the extrinsic and intrinsic pathways as shown in figure 2.

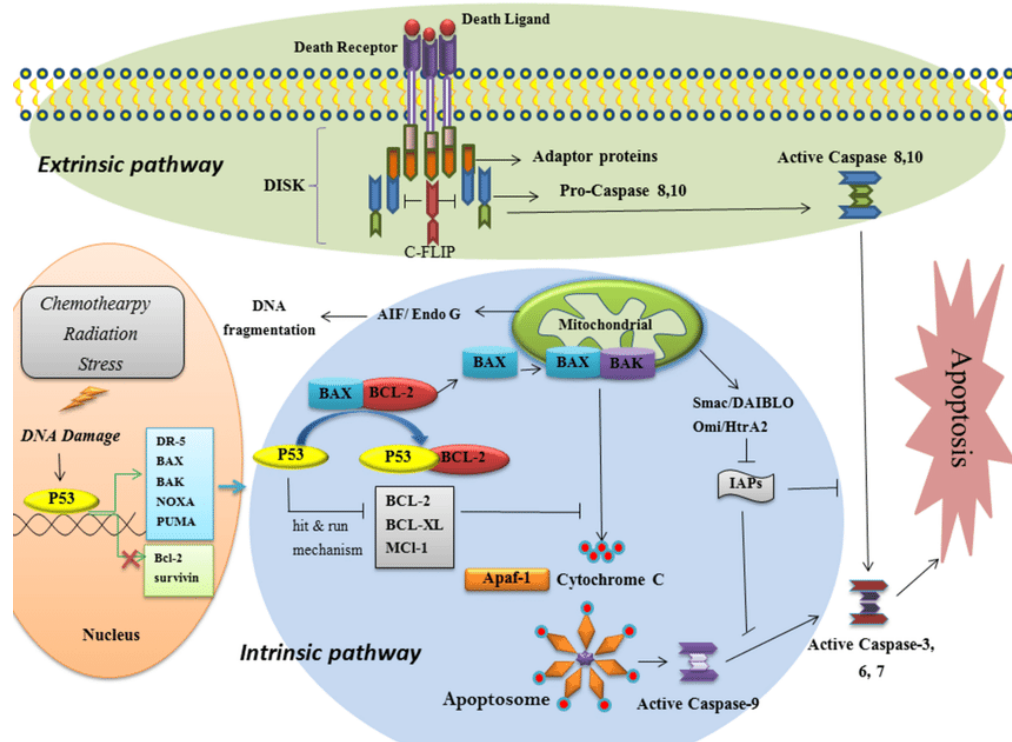


Figure 2 Extrinsic and intrinsic apoptotic signaling pathways (35)

In brief, extrinsic pathway activation occurs in response to ligation of the so-called death receptors, which are CD95 (also known as FAS), tumour necrosis factor receptor 1 or TNF-related apoptosis-inducing ligand receptor (TRAILR). The binding between ligand and death receptor results in the recruitment of several proteins, including FAS-associated death domain (FADD), TNFR1-associated death domain (TRADD), and caspase-8. The activated caspase-8 proteolytically activates downstream effector caspases or truncates the BH3 (Bcl-2 homology 3)-only protein

BID (BH3-interacting domain death agonist), which co-activates the intrinsic pathway of apoptosis by translocating to mitochondria (36).

Another pathway, intrinsic pathway is triggered by internal stimuli such as genetic damage, and severe oxidative stress resulted in mitochondrial outer membrane permeabilization (MOMP), which results in the release of cytochrome c from the mitochondrial intermembrane space. Cytosolic cytochrome c then triggers the assembly of a caspase-activating complex which are caspase-9 and apoptotic protease-activating factor 1 (APAF1; the apoptosome). Moreover, MOMP can be triggered by the activation of BH3-only proteins following their mobilization from other subcellular compartments and their post-translational modification (such as phosphorylation or proteolysis) or transcriptional upregulation (for instance in response to p53 activation) (37). BH3-only proteins generally stimulate MOMP by inducing the oligomerization of Bcl-2-associated X protein (BAX) and/or Bcl-2 antagonist or killer (BAK) in the outer mitochondrial membrane, thereby forming supramolecular channels that mediate the liberation of soluble proteins from the mitochondrial intermembrane space (38). DNA damage can stimulate the transactivation of genes encoding pro-apoptotic proteins (such as the BH3-only proteins p53 upregulated modulator of apoptosis (PUMA) and NOXA) by p53 or activate caspase-2 in a p53-dependent manner. Caspase-2 may then induce MOMP and/or activate other caspases, such as caspase-3, directly. Among the mitochondrial proteins that are released as a result of MOMP, apoptosis-inducing factor (AIF) and

endonuclease G (EndoG) can promote caspase-independent cell death (39). The majority of anticancer drugs currently used in clinical oncology use intact apoptotic signaling pathways to cause cancer cell death. As a result, defects in the death pathways can lead to drug resistance, limiting the efficacy of therapies. As a result, a better understanding of the apoptotic cell death signaling pathways may improve cancer therapy efficacy and circumvent resistance.

Role of p53 in apoptosis

In 50% of human cancers, the tumor suppressor gene *TP53* is mutated. Moreover to its function in tumor suppression, p53 is important in the response of malignant and nontransformed cells to many anticancer therapeutics, particularly those that cause DNA damage (40). The p53 protein plays a central role in apoptosis, and its inactivation may be the most frequent method of circumventing apoptosis in tumors. This protein has two other family members, p63 and p73 which appear to be involved in cancer development while p53 has a mechanism to prevent cancer formation (41, 42). Its activation by various extrinsic or intrinsic factors may result in many responses including senescence, cell cycle arrest, DNA repair, differentiation, and apoptosis.

p53 functions as an apoptotic regulator, modulating key control points in both the extrinsic and intrinsic pathways. Under normal conditions, p53 expression is

extremely low due to proteasomal degradation mediated primarily by the RING-finger type E3 ubiquitin protein ligase MDM2. When DNA is damaged cause p53 accumulation in the cell nucleus through post-translational modifications such as phosphorylation, acetylation and S-nitrosylation. These chemical modifications convert p53 from a dormant to an active state, which may be due to MDM2 dissociation from p53. Dutifully p53 is functionally active, it transactivates a specific set of target genes to induce cell cycle arrest and/or apoptosis, depending on the extent and type of DNA damage. When cells suffer from severe DNA damage, p53 uses its pro-apoptotic function to eliminate the cells and thus prevent the transfer of damaged DNA to daughter cells. As a result, p53 can maintain genomic integrity.

One of the most importance researched aspects of p53 research is its ability to control apoptosis as shown in figure 3. Therefore, p53 can be activated by hypoxia, DNA damage, or aberrant oncogene expression to induces DNA repair, cell-cycle checkpoints, cellular senescence, and apoptosis. p53 is a transcription factor that can bind DNA in a sequence-specific manner. The proapoptotic activity of p53 has been linked to its transactivation capabilities through several approaches. The ability of p53 can directly activate the transcription of proapoptotic members of the Bcl-2 family.

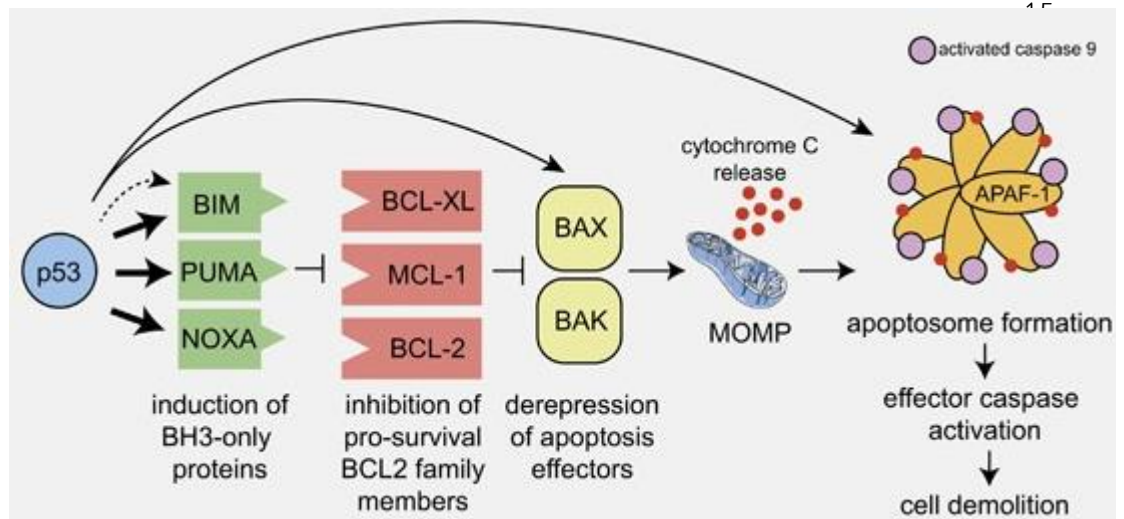


Figure 3 Mechanisms of p53-induced apoptosis (40)

p53 induces apoptosis in nontransformed cells mostly by direct transcriptional activation of the pro-apoptotic BH3-only proteins PUMA and NOXA. The BH3-only proteins bind and inhibit the pro-survival BCL-2 proteins (BCL-2, BCL-XL and MCL-1), thereby unleashing the cell death effectors BAX and BAK. Activation of BAX/BAK causes mitochondrial outer membrane permeabilisation (MOMP), the point of no return in apoptosis signaling, with consequent activation of the cascade of aspartate-specific cysteine proteases (caspases; in this pathway initiated by caspase-9 and its activator APAF-1) (43) that induces cell death.

Structural stability of the p53 tetramer

Tetramer formation of p53 is essential for site-specific DNA binding, posttranslational modifications, and protein-protein interactions. p53 binds DNA as a homotetramer, and tetramerization is mediated by the C-terminal tetramerization

domain (TD), which allosterically regulates the DNA-binding activity of p53 and the structure of p53 tetramer show in figure 4 (44). Tetramerization also affects posttranslational modifications (PTMs) of p53. It can be modified by as many as 50 individual PTMs, including phosphorylation, acetylation, methylation, glycosylation, ubiquitylation, neddylation, sumoylation, nitration, and poly-ribosylation. These modifications mainly occur in the N- and C-terminal regions and regulate p53 activity and tetramerization (45). MDM2-mediated polyubiquitylation of p53 is also affected by p53's oligomeric status; however, tetramerization has little effect on its proteasome degradation (46). Taken together provide a molecular/biophysical understanding of the evident role of the C terminus in post-translational modification that regulates the transcriptional function of p53. Furthermore, the unstructured C terminus is able to facilitate contacts between the core DNA-binding domains of the tetramer.

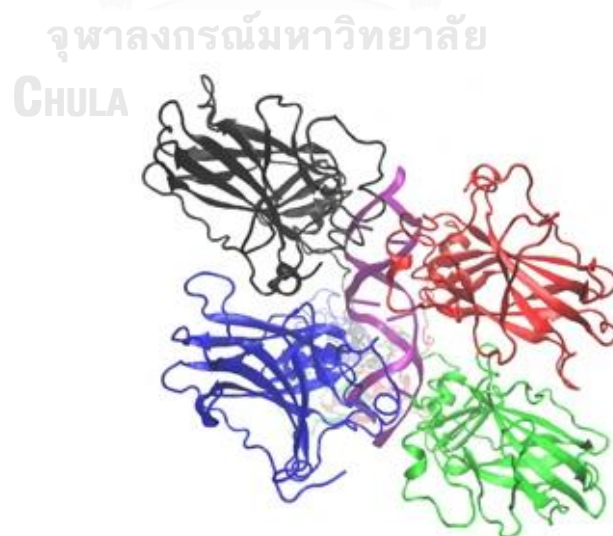


Figure 4 The 3D structure model of p53 tetramer (47)

Role of reactive oxygen species (ROS) in apoptosis induction

Several studies have indicated that reactive oxygen species (ROS) play a central role in the intracellular signaling pathway for a variety of cellular processes when they present at the low or moderate concentrations in normal condition (48). There are two distinct sources of ROS in the body, including mitochondrial respiratory chain and NADPH oxidase system. ROS are many kinds of molecules derived from oxygen that accepts electrons. When oxygen receives an electron, it forms the superoxide anion ($O_2^{\cdot-}$) that mainly produced from non-enzymatic process during oxidative phosphorylation of electron transport chain in mitochondria and from oxidation reaction of NADPH oxidase enzyme (49). Although, superoxide anion lacks on ability to penetrate liquid membranes, with accelerated by superoxide dismutases (SOD), the two molecules of the radical superoxide are converted to hydrogen peroxide (H_2O_2) which has a capability to penetrate cell membranes (50). Hydrogen peroxide may be partially reduced to hydroxyl radical (OH^{\cdot}) by receiving an electron or fully reduced to water by antioxidant enzymes. Hydroxyl radical is extremely reactive and cause cellular damage (51). In addition, superoxide anion can react with nitric oxide (NO) to produce peroxynitrite ($ONOO^-$) (52). Superoxide anion, hydroxyl radical and peroxynitrite cause damage cellular proteins, lipids and nucleic acids, which can lead to demise of the cell by apoptosis (18).

At lower doses, ROS such as H_2O_2 have been linked to induction of cell survival responses, whereas higher doses activate death processes such as apoptosis.

At lower doses, ROS activate the tumor suppressor protein p53 (53). p53 plays a key role in the control of cellular stress responses, inducing either cell cycle arrest to promote DNA repair and survival, or cell death by apoptosis, depending on the context (Figure 5). Under normal conditions, p53 has a short lifetime and is maintained at low levels through ubiquitination by Mdm2, leading to its proteasomal degradation. When the cell faces stress conditions or DNA damage, p53 is released from Mdm2 and stabilised by post-translational modifications, thus avoiding proteasomal degradation, before associating with DNA (54). If the stress is low, p53 induces cell cycle arrest, DNA repair and senescence. However if damage is too severe, p53 can regulate apoptosis transcriptionally by down-regulating pro-survival proteins such as Bcl-2, Bcl-XL, IAPs and survivin, and upregulating pro-apoptotic members (Figure 3) (53). p53 activates the transcription of pro-apoptotic genes that are crucial for inducing the intrinsic pathway of apoptosis, such as Bax, Bid, Puma, Noxa, and Apaf-1, and extrinsic pro-apoptotic factors such as Fas, FasL, DR-4, and DR-5 (40). Moreover, cytosolic p53 can translocate to mitochondria where it can interact directly with anti-apoptotic proteins such as Bcl-2, Bcl-XL, and Mcl-1 and the pro-apoptotic proteins Bax and Bak, which allow MOMP to release pro-apoptotic factors resulted in apoptosis (55). In addition, cytosolic p53 can activate Bax directly by causing its structural rearrangement (40). Thus p53 enhances mitochondrial membrane permeabilisation and subsequent release of pro-apoptotic factors from mitochondria, then induce apoptosis (55).

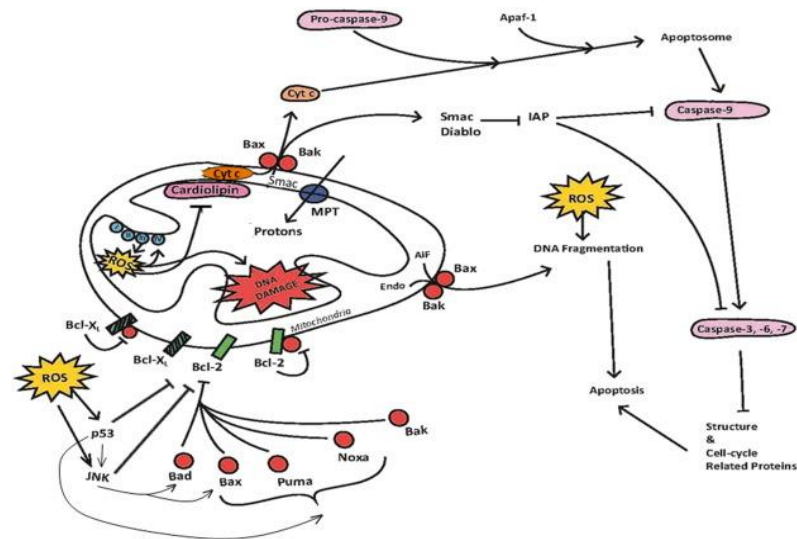


Figure 5 Activation of the mitochondrial (intrinsic) pathway of apoptosis by ROS (53)

ROS play a central role in cell signaling and in the regulation of the main pathways of apoptosis mediated by mitochondria, death receptors and the endoplasmic reticulum (ER). The deregulation of these different cell survival and cell death pathways is likely to have important pathological consequences for oxidative stress-associated diseases such as cancer and neurodegenerative diseases (53).

Advances in understanding of how different stress sensors such as ROS enable a switch from survival to death should lead to new strategies to prevent or treat some of these diseases.

Nitric oxide (NO) induce apoptosis

Nitric oxide (NO) is a water-soluble gas, which plays key role in various physiological as well as pathological processes. Role of NO has been first discovered as the mediator which regulates blood pressure and prevent cardiovascular diseases.

After that, NO has also been documented its role involving in immune system, nervous system, inflammation process, tumorigenesis and cancer progression. Effects of NO are mediated mainly via three routes (Figure 6) (56). Firstly, NO activation through cGMP signaling. cGMP is a second messenger cyclic nucleotide which is responsible for several cellular processes. NO stimulates cGMP by activating guanylyl catalase (sGC) which subsequently converses guanosine 5'-triphosphate (GTP) to cyclic guanosine 3', 5'-monophosphate (cGMP). This leads to formation of metal-nitrosyl complexes, and it may result in changes in the catalytic activity of the target enzyme. Secondly, S-nitrosylation reaction is a process to produce covalent bond between nitrogen monoxide and thiol group of cysteine residue in targeted protein. These processes occur in protein post-translational modification. After the S-nitrosylation, the conformation and properties of protein are changed which alter their biological function. Thirdly, a reaction of NO with superoxide anion results in a formation of peroxynitrite (ONOO^-) that is a strong oxidant and nitrating agent that is able to modify proteins, lipids and nucleic acids, which can lead to demise of the cell by apoptosis.

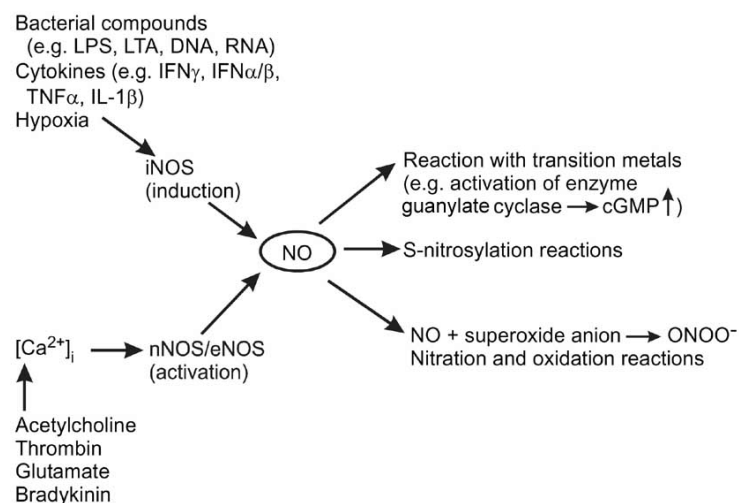


Figure 6 NO production and targets of NO-mediated signaling (56)

Reactive NO species such as peroxynitrite and dinitrogen trioxide can damage DNA and inhibit DNA repair mechanisms (57). p53 is an important tumor suppressor gene that is involved with induction of apoptosis and cell cycle regulation in cells that have sustained DNA damage. Peroxynitrite upregulated the expression of p53 which, in turn, resulted in increased expression of pro-apoptotic Bax and lower expression of antiapoptotic Bcl-2 (58). This data supports the hypothesis that peroxynitrite can contribute to the tumorigenic properties of p53 mutations. Peroxynitrite induces mitochondrial permeability transition changes and promotes apoptosis in cell-free systems containing mitochondria (59). These changes are hallmarks of cell death.

Crosstalk between ROS and NO in control of p53

The accumulating evidence suggests that both ROS and NO play important roles in apoptosis. These redox active small molecules can trigger cell death either independently or synergistically (34). Interestingly, many proteins are targets of both ROS and NO. Redox modification of amino acid residues is a key mechanism for controlling the expression and transcriptional activity of various transcription factors (60). Transcription factors subject to regulation by the redox status of the cell include NF κ B and AP-1, as well as p53. Different ROS and RNS give rise to modifications of

p53 and alter its activity (61). The NO modification of cysteine is important for the redox regulation of p53 function by *S*-nitrosylation that is, the coupling of an NO moiety to a reactive cysteine thiol (to form an *S*-nitrosothiol, SNO). Ubiquitylation and proteasomal targeting of the p53 protein is mediated by its interaction with human homologue of mouse double-minute-2 (HDM2), which is disrupted by *S*-nitrosylation of a critical Cys77 residue within HDM2, which results in increased p53 stability (62). The redox status of p53 is fundamentally important to its DNA-binding activity and affects to p53 conformation and oligomer formation. ROS activation of p53 through tetramerization is required for its tumor suppressive function by inducing transcriptional programs that lead to cell fate decisions such as cell cycle arrest or apoptosis. (63). Dimeric p53 variants are cytostatic and can arrest cell growth, but absence the capacity to trigger apoptosis in p53-null cells. On the other hand, p53 tetramers induce rapid apoptosis and cell growth arrest, while a monomeric variant is functionally inactive, supporting cell growth. Thus, indicates that alterations in the oligomerization status of p53 can influence the cell fate decisions between growth, arrest and apoptosis. Especially, the expression of pro-arrest *CDKN1A* and pro-apoptotic *P53AIP1* genes are essential cell fate determinants that are differentially regulated by the oligomeric state of p53 (64).

Various p53 gene mutations and polymorphisms have been reported, and the resulting changes in the p53 protein may affect intracellular localization and redox modification of the protein. The effects of this polymorphism, or others, on ROS

regulation of p53 would provide important insights into the effects of oxidative stress on p53 stabilization, localization and activity (65). Since mitochondria are the major source of ROS in the cell and ROS/NO can modify the activity of p53 it follows those alterations in mitochondrial functions that affect ROS/NO formation may also affect p53. In particular, changes in mitochondrial membrane potential (MMP) affect to p53 activity. p53 mitochondrial localization leads to decreased MMP and increased apoptosis (66). Thus, it is possible that ROS initiated in mitochondria may cause p53 translocation to mitochondria and enhance oxidative stress in mitochondria, thereby amplifying its apoptotic pathway.

Ti_{0.8}O₂ nanosheets

Nanotechnology is a branch of science that deals with tiny materials and their surfaces with dimensions <100 nm. Engineered nanoparticles (NPs) exhibit specific physicochemical characteristics and are manufactured for applications in several biological and commercial functions (67). In particular, nanotechnology when confronted with cancer biology has triggered new opportunities for improving targeted cancer therapy.

The main mechanism of NPs may result in oxidative stress or inflammatory responses that in turn have the potential to damage DNA and alter transcriptional patterns. NPs can be internalized into the cell by endocytosis then formation of

the endocytotic vesicles and release of particle ions from vesicles into the cell. The main factors responsible for ROS generation by NPs interaction with the mitochondria and/or NADPH oxidase and/or factors related to the physicochemical properties (size, shape, photoreactive properties, and surface chemistry) (68). These factors lead to ROS generation and its consequences, including DNA damage, cell cycle arrest, alterations in apoptosis, and damage to the cell membrane (Figure 7) (69).

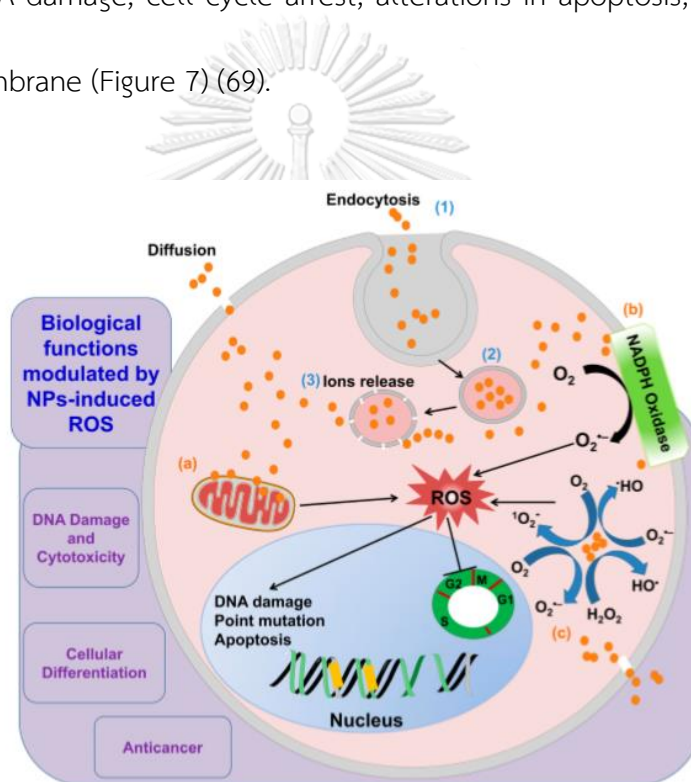


Figure 7 Schematic diagram describing the mechanisms implicated in

NP-induced ROS production (69)

Oxidative stress is a key factor involved in nanotoxicity, as well as in alterations to cell motility, cytotoxicity, unregulated cell signaling, DNA damage,

apoptosis, and cancer proliferations and metastasis (69). Additional oxidative stress from exposure to ROS-inducing agents leads to cell death due to toxicity induced by excess ROS production (70). In this regard, the ability of NPs to generate ROS could potentially be exploited for cancer therapy. In MCF-7 human breast cancer cells, Zn-doped TiO₂ NP exposure leads to drastic decreases in cell viability and increased cell cycle arrest associated with increases in oxidative stress (71). A previous study reported a role for p53 in cytotoxicity induced by zinc oxide NPs (72). In human hepatocarcinoma cells, oxidative stress mediated cell death induced by exposure to copper oxide NPs (73). The *in vivo* kinetics of nanoparticles is an essential to understand the hazard of nanoparticles. In previous study showed that the absorption, distribution, and excretion patterns of TiO₂ nanoparticles following oral administration were evaluated. TiO₂ nanoparticles had extremely low absorption and tissue distribution data showed that TiO₂ nanoparticles were not significantly increased in sampled organs (liver, kidney, spleen and brain). Ti concentration in the feces was very high compared to concentration in the urine or tissues. These results suggested that most of the nanoparticles were not absorbed from the gastrointestinal lumen (74).

In this study, we will focus on one of nanomaterials which is titania nanosheets (Ti_{0.8}O₂). Nanosheets are an emerging class of nanomaterial with two-dimensionality (2D) and interesting properties complementing their 1D or 0D analogs

(75). $\text{Ti}_{0.8}\text{O}_2$ nanosheets are an emerging 2D analog of TiO_2 and derived from the potassium zinc titanate precursor $\text{K}_{0.8}\text{Zn}_{0.4}\text{Ti}_{1.6}\text{O}_4$. The chemical exfoliation (i.e., soft chemistry) of the microcrystals can be easily performed on a large scale at room temperature, providing a stable aqueous colloid of negatively charged nanosheets. Their chemical compositions are derived from the microcrystals, while their lateral sizes can be controlled through exfoliating conditions (76). The surface engineering process modifies the 2D inorganic nanosheets planar surface with various functional motifs via chemical bonding or physical adsorption, which favors subsequent nanomedical applications in specific physiological environments, such as improved biostability, site-specific targeting capability, and multiple theranostic functions to facilitate oncological applications. While nanoparticles and nanotubes of TiO_2 have been extensively studied with regard to biomedical applications, (77) but studies on $\text{Ti}_{0.8}\text{O}_2$ nanosheets are limited. However, the mechanisms of anticancer activities of $\text{Ti}_{0.8}\text{O}_2$ nanosheets in NSCLC have not been elucidated yet. Therefore, $\text{Ti}_{0.8}\text{O}_2$ nanosheets anticancer mechanisms will be studied in this research. This study will evaluate effects of $\text{Ti}_{0.8}\text{O}_2$ nanosheets on NSCLC cell cytotoxicity through ROS generation and NO generation mediated apoptosis. Moreover, effect of $\text{Ti}_{0.8}\text{O}_2$ nanosheets on expression of p53 protein will also be observed because p53 is a nuclear transcription factor with a pro-apoptotic function. Activated p53 promotes cell cycle arrest to allow DNA repair and/or apoptosis to prevent the propagation of cells with serious DNA and p53-mediated therapeutic strategies to treat cancers.

Cancer treatment approaches based on nanomaterials

Targeted delivery is one of a major advantage of nanomaterial-based cancer therapy over free drugs. Targeted delivery based on nanoparticles has recently advanced. The idea of targeted delivery aiming for accuracy targeting of specific cancer cells, and it is achieved by either passive targeting or active targeting. Enhanced permeability and retention (EPR) effect is used in passive targeting while active targeting is achieved by conjugating with antibodies, peptides and small molecules. Compared with free drugs, targeted delivery helps reduce toxicity in normal cells (78). There are two main nanoparticles delivery methods: passive targeting and active targeting. When tumor grows, plenty of nutrition and oxygen are needed; in the meantime, tumor-induced angiogenesis generates many immature vasculatures that suppresses lymphatic drainage (79). These leaky blood vessels and cells membrane make it possible for chemical drugs to penetrate into cancerous sites. However, the size of drugs is crucial as regular particles are not small enough to percolate through cancerous cells. On the contrary, nanoparticles and related chemical drug vehicles can easily penetrate targeted sites and accumulate because of attenuated lymphatic drainages. A variety of molecules are found at different concentrations in normal cells compared to cancer cells due to abnormal gene expression and metabolism. These differences could be exploited for activation systems and can be separated into membrane proteins which are normally related with the over-expression of a gene and could enhance the penetration of

nanoparticles into the cell via internalization functionalities. The higher level of specific receptors on cancer cells surface compared to normal cells make it plausible to design functionalized nanoparticles that can specifically bind to these overexpressed receptors.

Strategies targeting cancer cells are a method to eliminate cancer. With EPR and active targeting, modified nanocarriers such as nanoparticles can reach cancer cells and release chemical drugs or biomaterials for killing to cancer cells. Nowadays, interactions between nanomaterials and cancer cells can occur via many mechanisms. Antigen-antibody conjugation modified nanoparticle endocytosis, liposome reaches cancerous area from blood vessels through EPR effect, the magnetic nanoparticle coated with chitosan carries 5-Fluorouracil. Under external magnetic field, the nanoparticle shows passive targeting ability at cancer cells (80).

MATERIALS AND METHODS

Chemicals

- Dimethyl sulfoxide from Sigma Chemical, Inc. (St. Louis, MO, USA).
- 3-(4,5-Dimethylthiazol-2-yl)-2,5-Diphenyltetrazolium Bromide (MTT) from Sigma Chemical, Inc. (St. Louis, MO, USA).
- Hoechst 33342 from Sigma Chemical, Inc. (St. Louis, MO, USA).
- Propidium iodide (PI) from Sigma Chemical, Inc. (St. Louis, MO, USA).
- Bovine serum albumin (BSA) from Sigma Chemical, Inc. (St. Louis, MO, USA).
- Dihydroethidium (DHE) from ImmunoTools (Friesoythe, Germany).
- Phosphate buffer saline (PBS) from GIBCO (Grand Island, NY, USA).
- Trypsin-EDTA from from GIBCO (Grand Island, NY, USA).
- Apoptosis kit (FITC) was purchased from ImmunoTools (Friesoythe, Germany).
- 2',7'-Dichlorofluorescein (DCF) from Invitrogen (Waltham, MD, USA).
- 3'-p-(hydroxyphenyl) fluorescein (HPF) from Invitrogen (Waltham, MD, USA).
- Mn(III)tetrakis (4-benzoic acid) porphyrin (MnTBAP) from Merck (Calbiochem, La Jolla, CA, USA).
- Antibodies from Cell Signaling Technology, Inc. (Danvers, MA, USA) for p53, Bcl-2, Mcl-1, Bax, caspase3, and β -actin, as well as peroxidase-conjugated secondary antibody
- RIPA buffer from Cell Signaling Technology, Inc. (Danvers, MA, USA)

- Pierce S-nitrosylation Western blot kits from Thermo Fisher Scientific (Calbiochem, La Jolla, CA, USA).

Test compound

The $\text{Ti}_{0.8}\text{O}_2$ nanosheets were prepared as reported previously. Briefly, the potassium zinc titanate $\text{K}_{0.8}\text{Zn}_{0.4}\text{Ti}_{1.6}\text{O}_4$ was first synthesized by heating the stoichiometric mixture of K_2CO_3 , ZnO , and TiO_2 at $900\text{ }^\circ\text{C}$ for 20 h. Then, the solid was soaked in 1 M HCl overnight (solid-to-solution ratio of 1 g to 100 mL) for a total of 3 cycles, with fresh acid replaced in between. The product is $\text{H}_{1.6}\text{Ti}_{1.6}\text{O}_4 \cdot 0.8\text{H}_2\text{O}$, where 0.8H^+ is first exchanged for 0.8K^+ , another 0.8H^+ for the leached (81) 0.4Zn^{2+} , with water inclusion. Finally, 0.4 of the protonic form was mechanically shaken at 180 rpm for 14 days with diluted tetrabutylammonium hydroxide (TBAOH) solution (1 M, Sigma-Aldrich, St. Louis, MO, USA). The solid-to-solution ratio was fixed at 0.4 g-to-100 mL and the TBA^+/H^+ ratio at 1. The white colloid of $\text{Ti}_{0.8}\text{O}_2$ nanosheets was then obtained.

The absorption characteristics of the nanosheets colloid were measured using a T90+ UV/VIS spectrometer (PG Instruments, Lutterworth, UK). The “size” of the nanosheets (i.e., the hydrodynamic radius, as determined by dynamic light scattering) and the zeta potential were measured using a Beckman Coulter Delsa Nano (Beckman Coulter Inc., Fullerton, CA, USA) instrument. The nanosheets were also imaged using a JEOL JEM 2010 (Beckman Coulter Inc., Fullerton, CA, USA)

transmission electron microscope. Other results can be found in more detail elsewhere.

Cell culture

H23, H292, H460, and A549 lung cancer cells were obtained from the American Type Culture Collection (Manassas, VA, USA). A primary human dermal papilla cell line (primary DP1) was purchased from Celprogen (Benelux, Netherlands). A human keratinocyte cell line (HaCaT) was purchased from Cell Lines Service (Heidelberg, Germany). Immortalized dermal papilla cells (DP) and human primary hair follicle dermal papilla cells (primary DP2) were purchased from Applied Biological Materials Inc (Richmond, BC, British Columbia). H460, H292, and H23 cells were cultured in RPMI 1640 medium (Gibco, Grand Island, NY, USA), whereas A549, HaCaT, DP, and primary DP1 and DP2 cells were cultivated in DMEM medium (Gibco, Grand Island, NY, USA). The medium was supplemented with 10% fetal bovine serum (FBS), 100 units/mL penicillin/streptomycin, and 2 mM L-glutamine (Gibco, Waltham, MD, USA). The cells were incubated in a 5% CO₂ environment at 37 °C.

Patient-derived primary lung cancer cell line preparation from malignant pleural effusion

The patient-derived lung cancer cells were prepared from pleural effusion of recurrent or advanced stage non-small cell lung cancer patients at the King Chulalongkorn Memorial Hospital. The Ethics Committee of the Faculty of Medicine,

Chulalongkorn University, Bangkok, Thailand (IRB 581 365/62) approved the protocol. Informed consent from all contributors was obtained. Pleural effusion (approximately 1000 mL) was collected through thoracentesis. The samples were centrifuged at 300x g for 10 min. The cells were cultured in RPMI medium with 10% FBS, 2 mM L-glutamine, and 100 units/mL each of penicillin and streptomycin.

Methodes

1. Cytotoxicity assay

Cells were seeded onto 96-well plates at the density of 1×10^4 cells/well and were allowed to incubate overnight. Then, cells were treated with various concentrations (0–100 $\mu\text{g/mL}$) of $\text{Ti}_{0.8}\text{O}_2$ nanosheets for 24 h at 37 °C and analyzed for cell viability using a 3-(4,5-dimethylthiazol-2-yl)-2,5-diphenyltetrazolium bromide (MTT) assay. The MTT product was measured at 570 nm using a microplate reader. Cell viability was calculated by dividing the absorbance of the treated cells by that of the control cells and represented in percentage. All analyses were performed in 3 independent replicate cell cultures.

2. Nuclear staining assay

To determine apoptotic and necrotic cell death, H460 and A549 cells were seeded onto 96-well plates at the density of 1×10^4 cells/well, incubated overnight, and then treated with $\text{Ti}_{0.8}\text{O}_2$ nanosheets at various concentrations (0–

10 $\mu\text{g}/\text{mL}$) for 24 h at 37 °C. After that, the cells were incubated with Hoechst 33342 (10 $\mu\text{g}/\text{mL}$) and propidium iodide (PI) (5 $\mu\text{g}/\text{mL}$) for 30 min at 37 °C in the dark. These cells were imaged under a fluorescence microscope (Nikon ECLIPSE Ts2, Tokyo, Japan).

3. Cell apoptosis analysis

The stages of apoptosis and necrosis cells were determined with annexin V-FITC apoptosis kits (ImmunoTools, Germany). H460 and A549 cells were seeded in 24-well plates at a density of 1×10^5 cells/mL and treated with $\text{Ti}_{0.8}\text{O}_2$ nanosheets at various concentrations (0–10 $\mu\text{g}/\text{mL}$) for 24 h. Then, the cells were detached and suspended in 100 μL of 1X binding buffer and incubated in 5 μL of annexin V-FITC and 1 μL of PI for 15 min at room temperature in the dark. Next, the cells were analyzed by guava easyCyte™ flow cytometry systems.

4. Scanning Electron Microscopy (SEM) morphological analysis

Cells were fixed in 2.5% glutaraldehyde in 0.1 M phosphate buffer (pH 7.2) for 2 h. Next, the cells were dehydrated with a graded series of ethanol (30%, 50%, 70%, and 95% for 5 min/each and 100% 3 times, 5 min/time), dried, mounted, and coated with gold (sputter coater, Balzers model SCD 040, Wetzlar, Germany). Finally, the cells were observed under SEM (JEOL, model JSM6400, Tokyo, Japan).

5. Transmission Electron Microscopy (TEM) for cellular uptake analysis

Cells were seeded at the density of 1×10^6 cells/mL and treated with $\text{Ti}_{0.8}\text{O}_2$ nanosheets at $10 \mu\text{g/mL}$ for 24 h. The cells were collected, washed with PBS, and fixed in 2% glutaraldehyde, post-fixed in 1% osmium tetroxide, dehydrated in alcohol, and embedded. Thin sections of the resin-embedded cells were cut and subjected to a JEM-1400 (Jeol Ltd., Tokyo, Japan) transmission electron microscope (TEM).

6. Western Blot analysis

After treatment, the cells were lysed, as previously described. Equal amounts of protein from each sample were subjected to SDS-PAGE for separation and transferred to nitrocellulose or PVDF membranes (Bio-Rad, Hercules, California, USA). The blots were blocked for 1 h. with 5% non-fat dry milk [20] and, after that, incubated with specific primary antibodies against p53, Bcl-2, Mcl-1, Bax, caspase 3, and β -actin at 4°C overnight. Then, the blots were washed in TBST and incubated with horseradish peroxidase (HRP)-conjugated secondary antibodies for 2 h at room temperature. Finally, protein bands were detected using an enhanced chemiluminescence substrate (Supersignal West Pico; Pierce, Rockford, IL, USA) and exposed to film.

7. ROS, superoxide anion, and hydroxyl radical detection by flow cytometry

A549 and H460 were seeded in 24-well plates and cultured for 12 h. DCFHDA, DHE, and HPF were added, and the cells were incubated for 30 min in

the dark. Cells were treated with $\text{Ti}_{0.8}\text{O}_2$ nanosheets for 3 h, washed, and resuspended in PBS. DCF fluorescence was quantified using guava easyCyte™ flow cytometry systems.

8. NO detection by DAF-FM DA assay

After detachment, the cells were collected and incubated with 10 μM DAF-FM DA for 30 min at 37 °C. The cells were then washed, resuspended in phosphate-buffered saline, and analyzed for fluorescence intensity using guava easyCyte™ flow cytometry systems. These cells were imaged under a fluorescence microscope (Nikon ECLIPSE Ts2).

9. Immunofluorescence

Cells were seeded onto 96-well plates at the density of 1×10^5 cells/well. The cells were treated with a nanosheet and fixed with 4% (w/v) paraformaldehyde for 30 min. The cells were permeabilized with 0.1% (v/v) Triton-X for 20 min, incubated with 3% (w/v) BSA for 30 min, and washed and incubated with a p53 antibody overnight at 4 °C. The cells were washed and incubated with Alexa Fluor 488 conjugated secondary antibodies for 1 h at room temperature. The cells were washed with PBS, co-stained with 10 $\mu\text{g}/\text{mL}$ Hoechst 33342, and visualized under a fluorescence microscope (Nikon ECLIPSE Ts2).

10. Cycloheximide (CHX) chasing assay

Cells were seeded and treated with 10 $\mu\text{g}/\text{mL}$ of $\text{Ti}_{0.8}\text{O}_2$ nanosheets with or without 50 $\mu\text{g}/\text{mL}$ CHX for 0, 15, 30, 45, 60, and 90 min. The cells were lysed with RIPA lysis buffer containing the protease inhibitor cocktail (Roche Diagnostics, Indianapolis, IN, USA). Western blot analysis was performed for detecting p53 protein levels. Protein bands were analyzed using ImageJ software (version 1.52, National Institutes of Health, Bethesda, MD, USA), and the Mcl-1 protein half-life was calculated.

11. Immunoprecipitation assay

Cells were treated with $\text{Ti}_{0.8}\text{O}_2$ nanosheets for 1 h. Immunoprecipitation was performed using Dynabeads™ Protein G immunoprecipitation kits from Thermo Fisher Scientific Inc (Waltham, MA, USA). Magnetic beads were prepared and incubated with the p53 antibody for 20 min. A bead-Ab complex was mixed with cell lysate and incubated at 4 °C overnight. The bead-Ab-Ag complex was washed three times, separated on a magnet between each wash, and the supernatant was removed. Elution buffer was added. The supernatant was then subjected to Western blot analysis.

12. S-Nitrosylated protein detection

Cells were lysed and centrifuged at 10,000 $\times g$ for 10 min. To each sample, 2 μL of 1 M MMTS was added, and the samples were incubated for 30 min at room temperature to block free cysteine thiols. Then, the protein was precipitated by

adding pre-chilled ($-20\text{ }^{\circ}\text{C}$) acetone and freezing at $-20\text{ }^{\circ}\text{C}$ to remove MMTS for at least 1 h. Samples were centrifuged at $10,000\times g$ for 10 min at $4\text{ }^{\circ}\text{C}$. Pellets were resuspended in $100\text{ }\mu\text{L}$ of HENS buffer, $1\text{ }\mu\text{L}$ of the labeling reagent, and $2\text{ }\mu\text{L}$ of 1M sodium ascorbate for 1–2 h at room temperature. Finally, labeled-protein SDS-PAGE and Western blotting analysis were used to detect S-nitrosylation p53 proteins.

13. Computational method

The X-ray structure of the tetrameric p53 core domain was taken from the Protein Data Bank (PDB ID: 3KMD) (82). The H++ web server (83) was used to assign the protonation state of all ionizable groups of amino acids at pH 7.4. The modeled protein was then submitted to all-atom molecular dynamics (MD) simulations using the AMBER16 software package according to standard procedures (84-86), as summarized below. In brief, the starting structure of the p53 protein was firstly energy-minimized using the steepest descent (500 steps) and a conjugated gradient (1500 steps) based on the ff14SB AMBER force field (87) to reduce unfavorable contacts. After that, a 100-ns MD simulation with the NPT ensemble at 310 K and 1 atm was carried out by the PMEMD module of AMBER16. The SHAKE algorithm (88) was applied to restrain the covalent bond involved in hydrogen atoms, allowing a simulation time step of 2 fs. The particle mesh Ewald (89) summation method was used to treat the long-range electrostatic

interactions, whereas a nonbonded cutoff distance was set to 10 Å. The MD trajectories in the production phase were collected every 10 ps and analyzed in terms of intermolecular hydrogen bonding interaction using the CPPTRAJ module (90) of AMBER 16. To determine the essential residues associated with protein–protein binding at the interface of the four monomers and the effect of S-nitrosylation on the cysteine (Cys) residue towards protein stability, the per-residue decomposition free energy ($\Delta G_{\text{bind}}^{\text{residue}}$) method, based on the molecular mechanics/Poisson-Boltzmann surface area (MM/PBSA), was performed using the MMPBSA.py module (91) implemented in AMBER16.

Statistical analysis

Data from three independent experiments are presented as mean \pm standard error of mean (SEM). Multiple comparisons for statistically significant differences between multiple groups were performed using analysis of variance (ANOVA), followed by Turkey's post hoc test. *P*-values <0.05 were considered statistically significant.

RESULTS

1. Cytotoxicity of the $Ti_{0.8}O_2$ nanosheets on human lung cancer cells and normal cells

Cells were treated with various concentrations of $Ti_{0.8}O_2$ nanosheets (0–100 $\mu\text{g/mL}$) for 24 h using and analyzed by MTT assay. The results revealed the statistically significant cytotoxic effects of the $Ti_{0.8}O_2$ nanosheets occurred at concentrations of 10–100 $\mu\text{g/mL}$ in A549, H460, and H23 cells and at 20–100 $\mu\text{g/mL}$ in H292 cells (Figure 8), data are shown as the mean \pm SEM ($n = 3$). * $p < 0.05$ versus non-treated control.

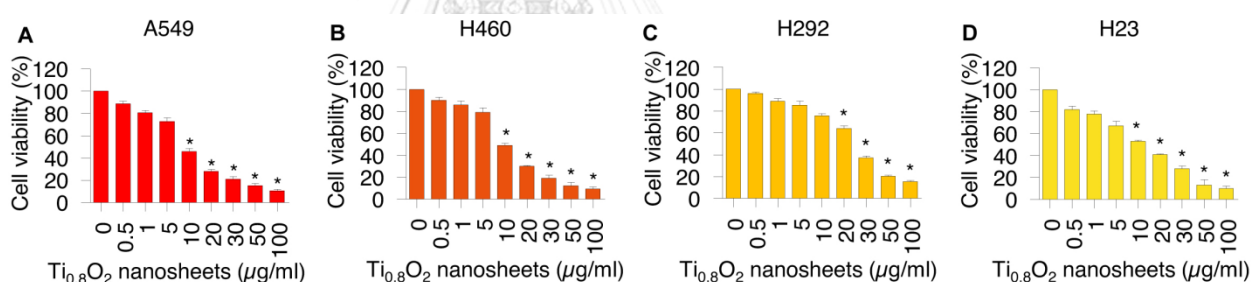


Figure 8 Effect of $Ti_{0.8}O_2$ nanosheets on cell viability of lung cancer cells

In the normal cells, primary dermal papilla cells from different sources (DP1 and DP2), cytotoxic effects of the $Ti_{0.8}O_2$ nanosheets were found at 50 $\mu\text{g/mL}$. Moreover, at the concentration of 30 $\mu\text{g/mL}$, the $Ti_{0.8}O_2$ nanosheets showed statistically significant cytotoxic effects on DP and HaCat cells (Figure 9).

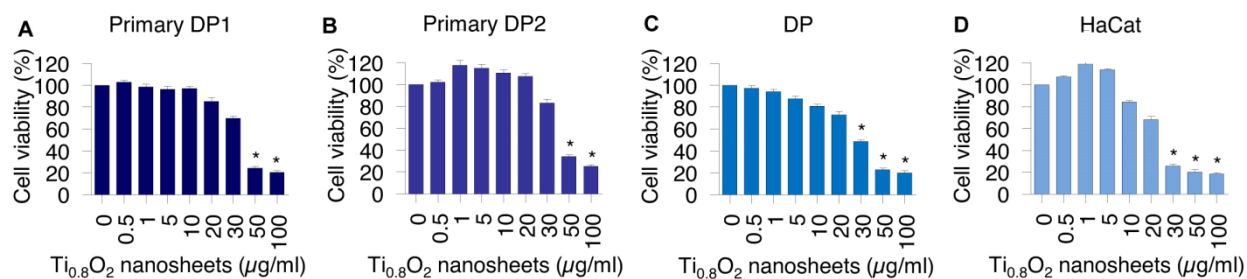


Figure 9 Effect of $Ti_{0.8}O_2$ nanosheets on cell viability of normal cells

2. Effect of $Ti_{0.8}O_2$ nanosheets on apoptosis in human lung cancer cells

Characteristic apoptosis cells were identified using a nuclear staining assay.

Morphology of apoptotic nuclei stained with Hoechst 33342 dye and propidium

iodide in cells treated with $Ti_{0.8}O_2$ nanosheets, determined by visualization using

fluorescence microscopy and calculated percentages of nuclear fragmented and PI-

positive cells. The results showed that the $Ti_{0.8}O_2$ nanosheets mediated apoptosis in

lung cancer cells at concentrations of 1–10 $\mu\text{g/mL}$, with a small percentage of

necrotic cells (Figure 10), data are shown as the mean \pm SEM ($n = 3$). * $p < 0.05$ versus

non-treated control.

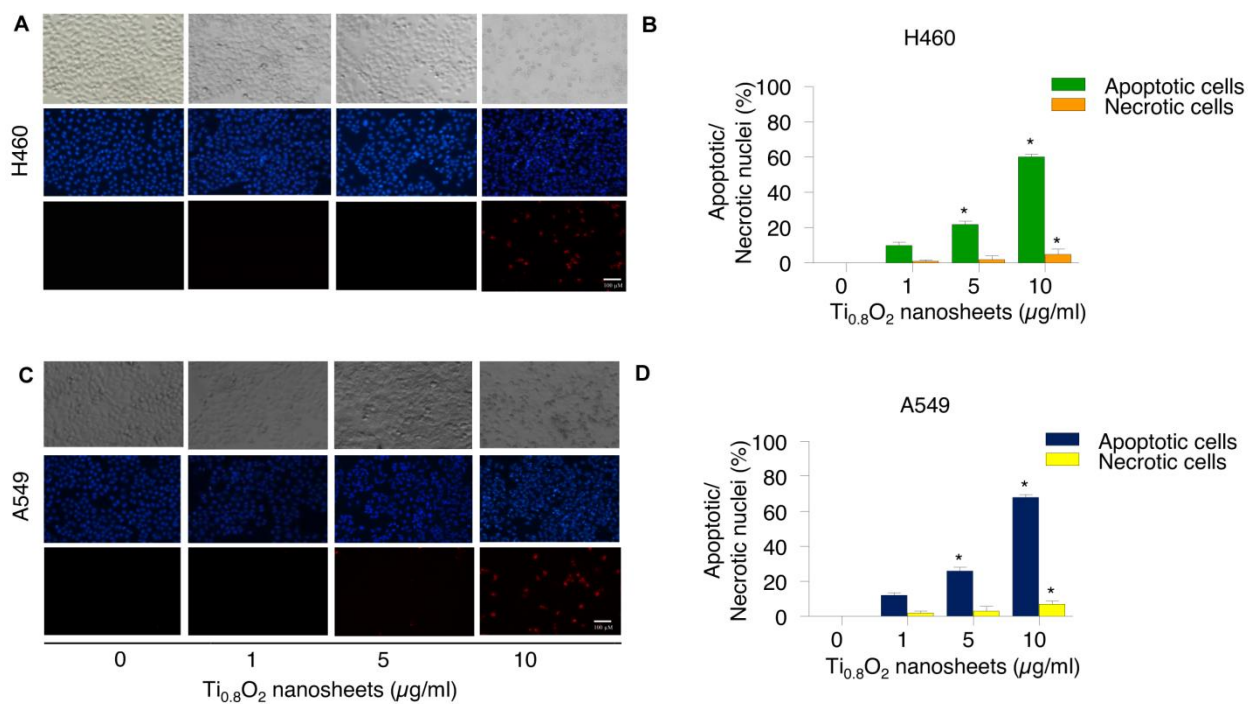


Figure 10 Effect of Ti_{0.8}O₂ nanosheets on characteristic apoptosis cells by a nuclear staining assay

Apoptotic and necrotic cells were determined using annexin V-FITC/PI staining with flow cytometry. Flow cytometry analysis based on annexin V/PI detection also confirmed that 10 µg/mL of Ti_{0.8}O₂ nanosheets induced dramatic apoptosis in A549 and H460 cells compared with untreated cells (Figure 11), data are shown as the mean ± SEM (*n* = 3). * *p* < 0.05 versus non-treated control.

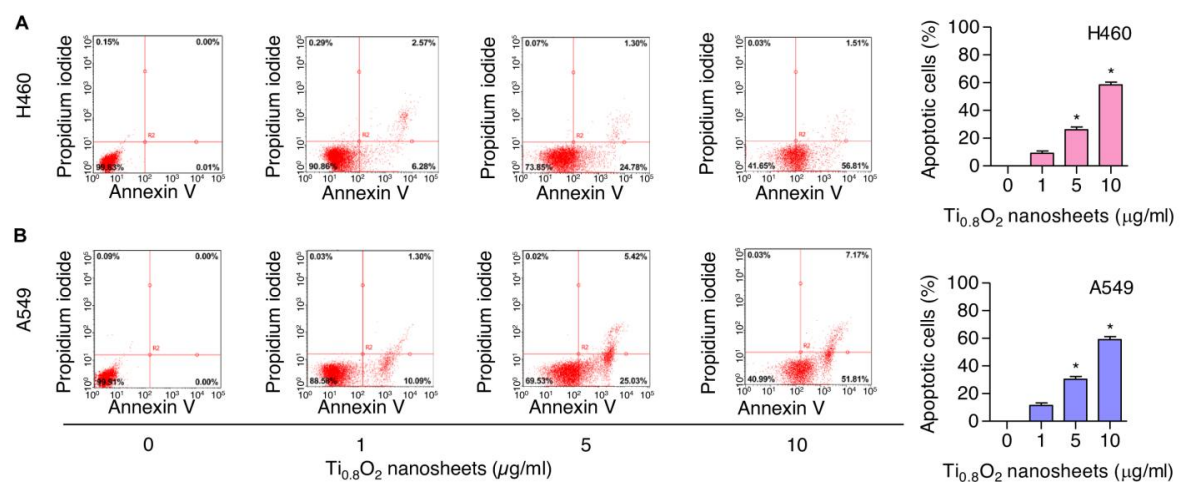


Figure 11 Effect of $Ti_{0.8}O_2$ nanosheets on characteristic apoptosis cells by annexin V-FITC/PI staining with flow cytometry

3. Uptake of the $Ti_{0.8}O_2$ nanosheets by cancer cells

Morphology of H460 cells determined by scanning electron microscopy (SEM).

Cellular uptake of $Ti_{0.8}O_2$ nanosheets in H460 and primary DP cells at 24 h, determined by transmission electron microscopy (TEM). Under SEM morphological analysis, it was seen that for H460 cells, the morphology of the cancer cells gradually changed when treated with $Ti_{0.8}O_2$ nanosheets at concentrations of 1–10

$\mu\text{g/mL}$ (Figure 12).

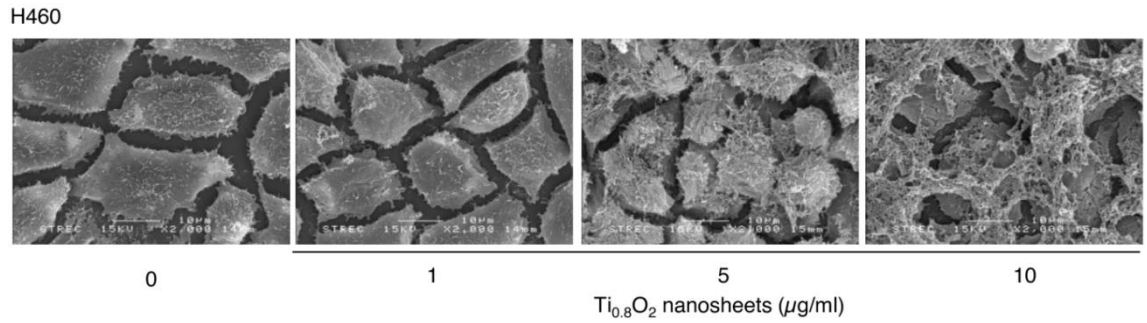


Figure 12 Morphology of H460 cells determined by scanning electron microscopy (SEM)

Moreover, cellular uptake by TEM analysis showed that $\text{Ti}_{0.8}\text{O}_2$ nanosheets at 10 $\mu\text{g/ml}$ could appropriately pass into the H460 cells more than primary DP cells (Figure 13).

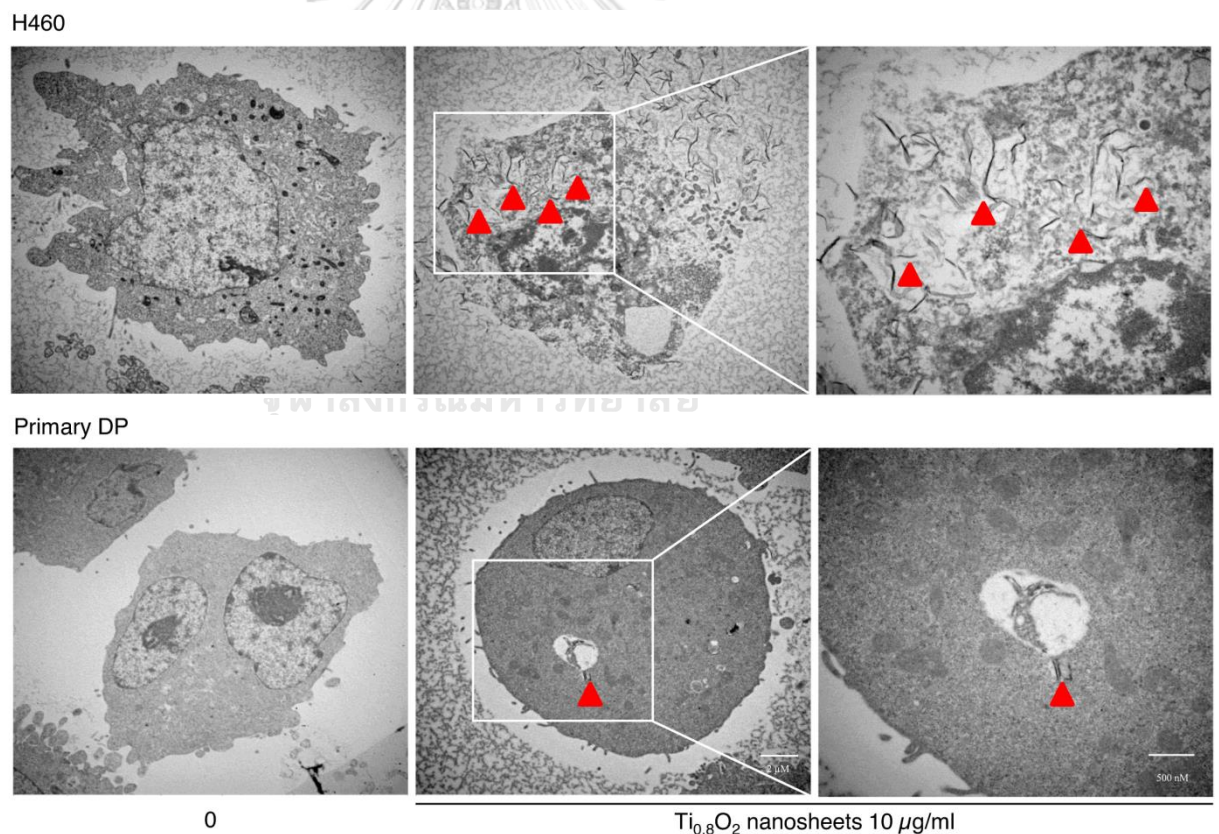


Figure 13 Cellular uptake of $\text{Ti}_{0.8}\text{O}_2$ nanosheets in H460 and primary DP cells at 24 h

by transmission electron microscopy (TEM)

4. $Ti_{0.8}O_2$ nanosheets modulate apoptosis-related proteins in H460 and A549 cells

In order to investigate the mechanism of $Ti_{0.8}O_2$ nanosheet-induced apoptosis, the apoptotic-related proteins were determined by Western blot analysis. A549 and H460 cells were treated with 0–10 $\mu\text{g/mL}$ $Ti_{0.8}O_2$ nanosheets, and then the pro-and anti-apoptotic proteins related to mitochondria-mediated apoptosis were evaluated, data are shown as the mean \pm SEM ($n = 3$). * $p < 0.05$ versus non-treated control. The results showed that the $Ti_{0.8}O_2$ nanosheets increased the pro-apoptotic protein Bax, whereas the anti-apoptotic proteins Mcl-1 and Bcl-2 were downregulated in the cells treated with the $Ti_{0.8}O_2$ nanosheets. In addition, procaspase3 decreased in a concentration-dependent manner. Moreover, $Ti_{0.8}O_2$ nanosheets caused a significant increase in p53 protein levels in a dose-dependent manner (Figure 14A–D). These findings suggest that p53 may play a role in $Ti_{0.8}O_2$ nanosheet-induced apoptosis of NSCLC cells. Taken together, it can be concluded that the $Ti_{0.8}O_2$ nanosheets mediated the apoptosis of lung cancer cells by increasing pro-apoptotic proteins, which led to cell death by the mitochondria-dependent pathway.

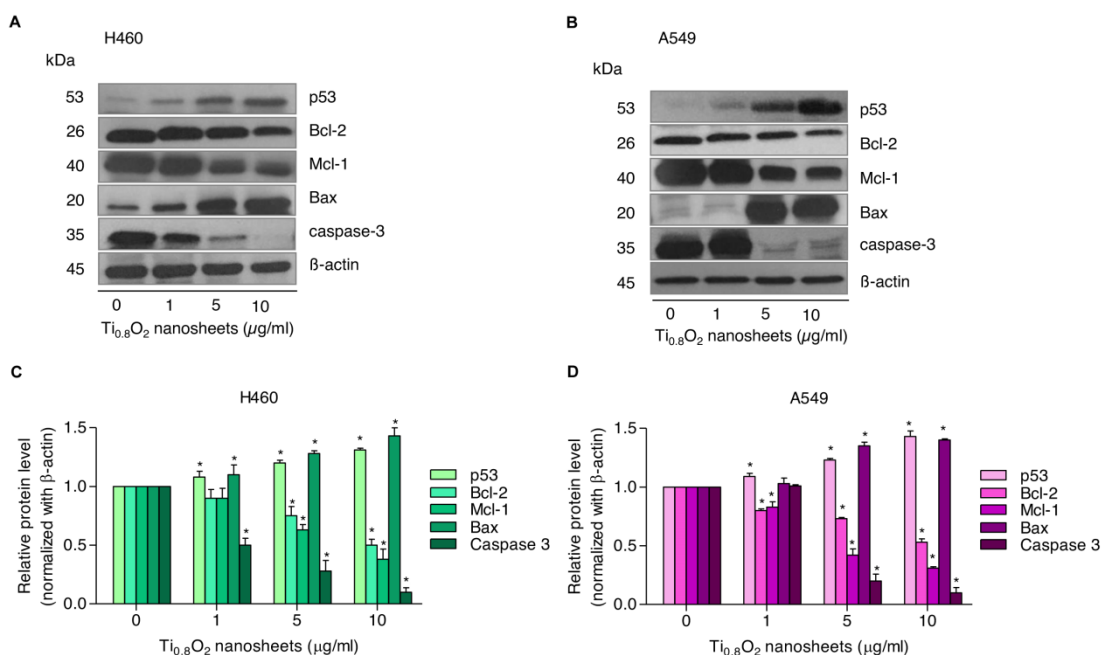


Figure 14 Effect of Ti_{0.8}O₂ nanosheets on apoptosis-related proteins

5. Cytotoxicity and apoptotic effects of Ti_{0.8}O₂ nanosheets on advanced lung cancer cells from patients

To assess the potential pharmacological activities of synthetic Ti_{0.8}O₂ nanosheet compounds in advanced lung cancer cells, treatment with current standard therapeutic agents was also performed for comparison. Two groups of cell lines were used for the investigations: Panel A, an advanced non-small cell lung cancer cell line from patients with malignant pleural effusion who had never been treated by chemotherapy, targeted therapy, or immunotherapy, and Panel B, an advanced non-small cell lung cancer cell line from patients with malignant pleural effusion who had been treated with standard platinum-doublet chemoRx with or without targeted therapy or a checkpoint inhibitor and second-line chemoRx. In total, four primary lung cancer cells were treated with the same concentrations of Ti_{0.8}O₂

nanosheets, cisplatin, and etoposide (0–100 $\mu\text{g}/\text{mL}$) for 24 h and subjected to cell viability analysis by MTT assay. The $\text{Ti}_{0.8}\text{O}_2$ nanosheets could be considered nontoxic at doses lower than 1 $\mu\text{g}/\text{mL}$, while a concentration of more than 5 $\mu\text{g}/\text{mL}$ caused a significant decrease in the cell viability of the cells (Figure 15).

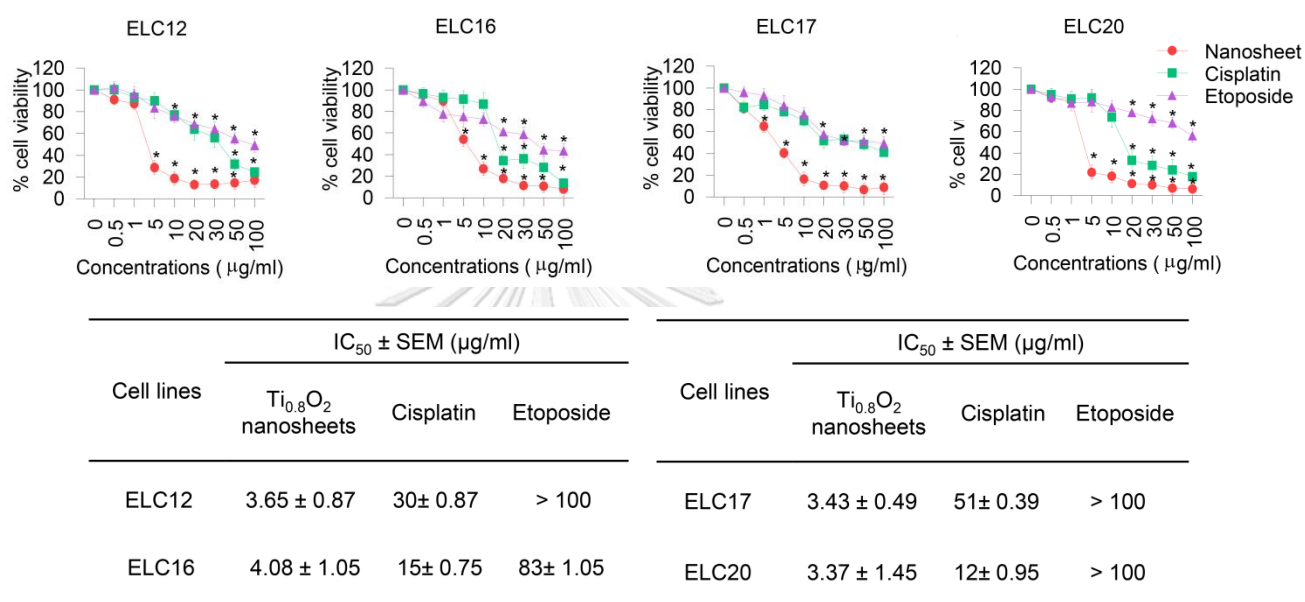


Figure 15 Cytotoxicity of the $\text{Ti}_{0.8}\text{O}_2$ nanosheets on malignant pleural effusion from advanced lung cancer patients

In contrast, the standard drugs showed slightly decreased cell viability from 0.5 to 100 $\mu\text{g}/\text{mL}$, while doses of more than 20 $\mu\text{g}/\text{mL}$ cisplatin and etoposide were considered toxic. Data analysis showed that the IC₅₀ of the $\text{Ti}_{0.8}\text{O}_2$ nanosheets was lower than 10 $\mu\text{g}/\text{mL}$ at 24 h, which was significantly lower than for cisplatin and etoposide. The results showed that the $\text{Ti}_{0.8}\text{O}_2$ nanosheets reduced cell viability in a concentration-dependent manner compared with the untreated controls (Figure 15).

To confirm the effect of the $Ti_{0.8}O_2$ nanosheets on advanced lung cancer cells from patients, a nuclear staining assay using Hoechst 33342 and propidium iodide was performed and the results analyzed. After treatment with the compounds at 10 $\mu\text{g}/\text{mL}$ of $Ti_{0.8}O_2$ nanosheets, apoptotic cells were observed by the presence of nuclear condensation morphology in the representative cell line (Figure 16). It was found that the potency of the nanosheets was dramatically higher than that of cisplatin and etoposide.

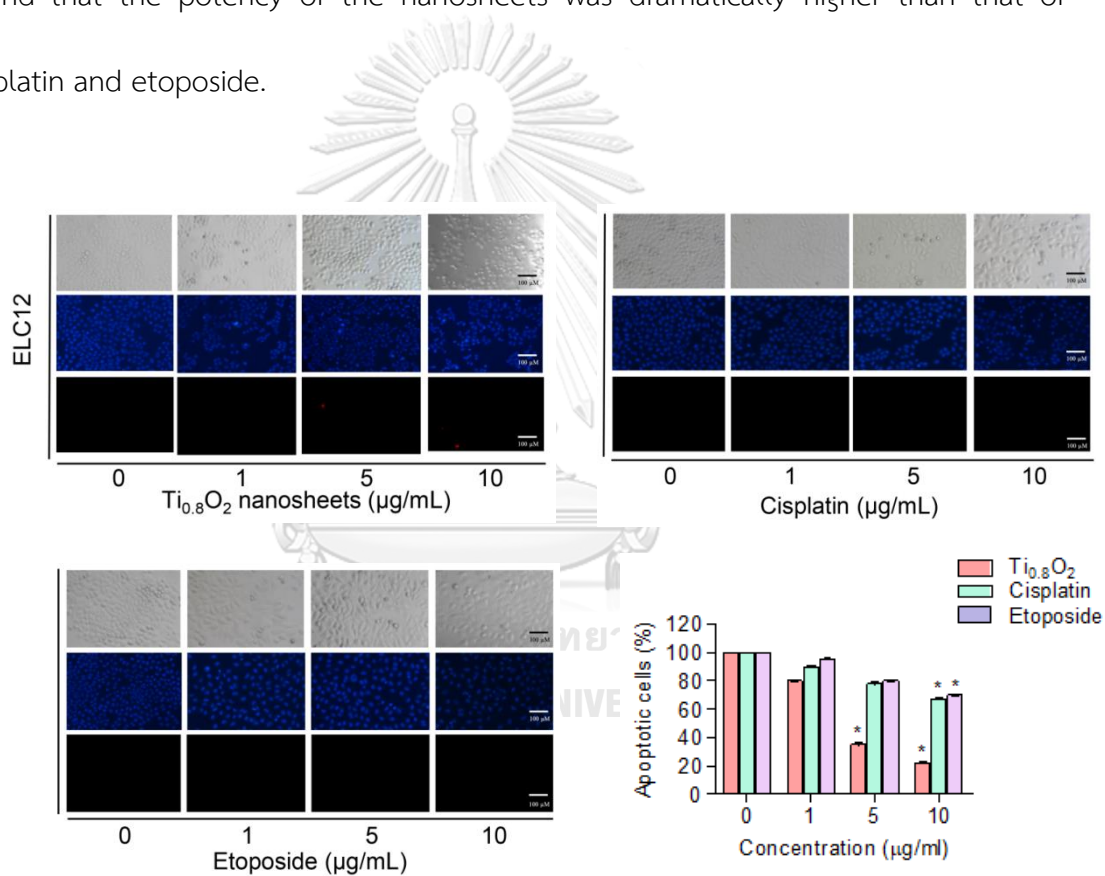
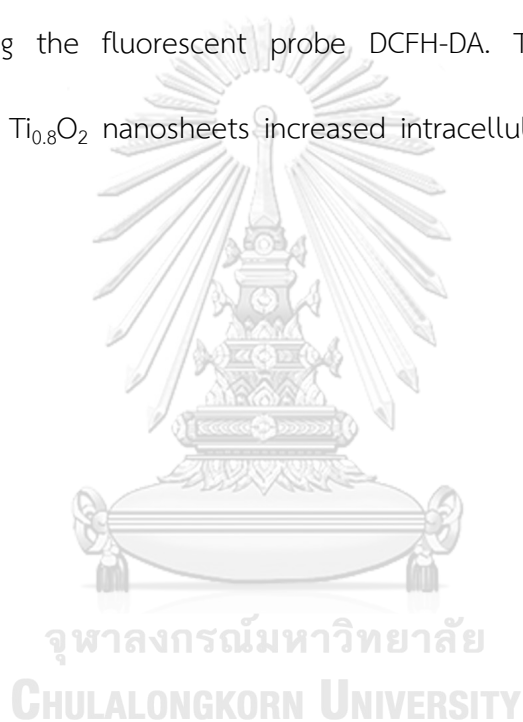


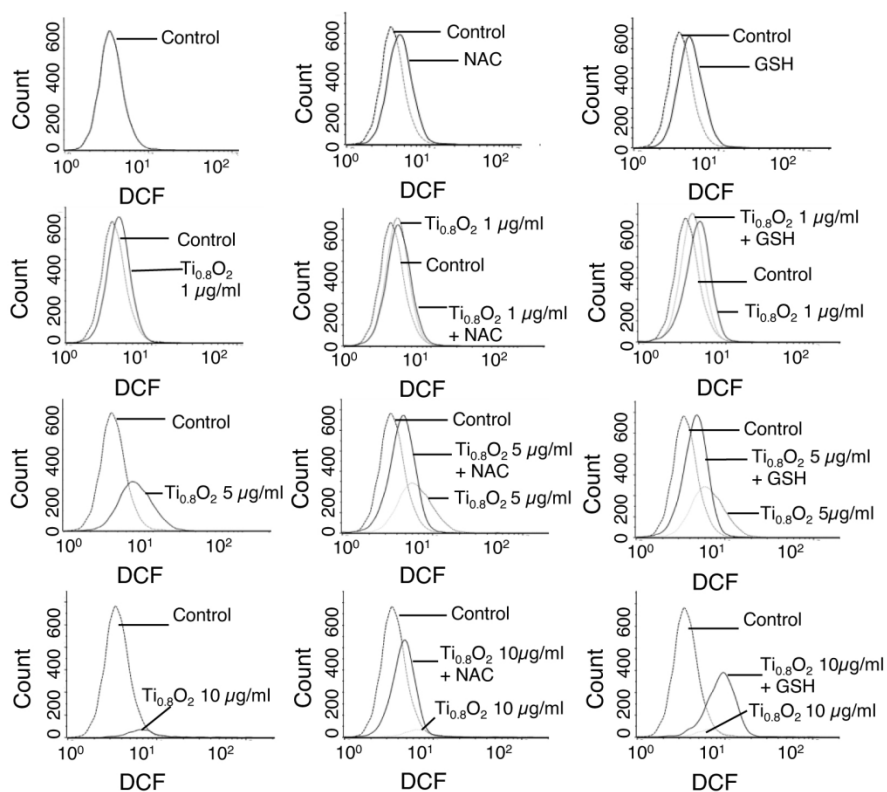
Figure 16 Effect of $Ti_{0.8}O_2$ nanosheets, Cisplatin and Etoposide on characteristic apoptosis cells by a nuclear staining assay of malignant pleural effusion from advanced lung cancer patients

6. Effect of $Ti_{0.8}O_2$ Nanosheets on intracellular ROS induction in A549 and H460 cells

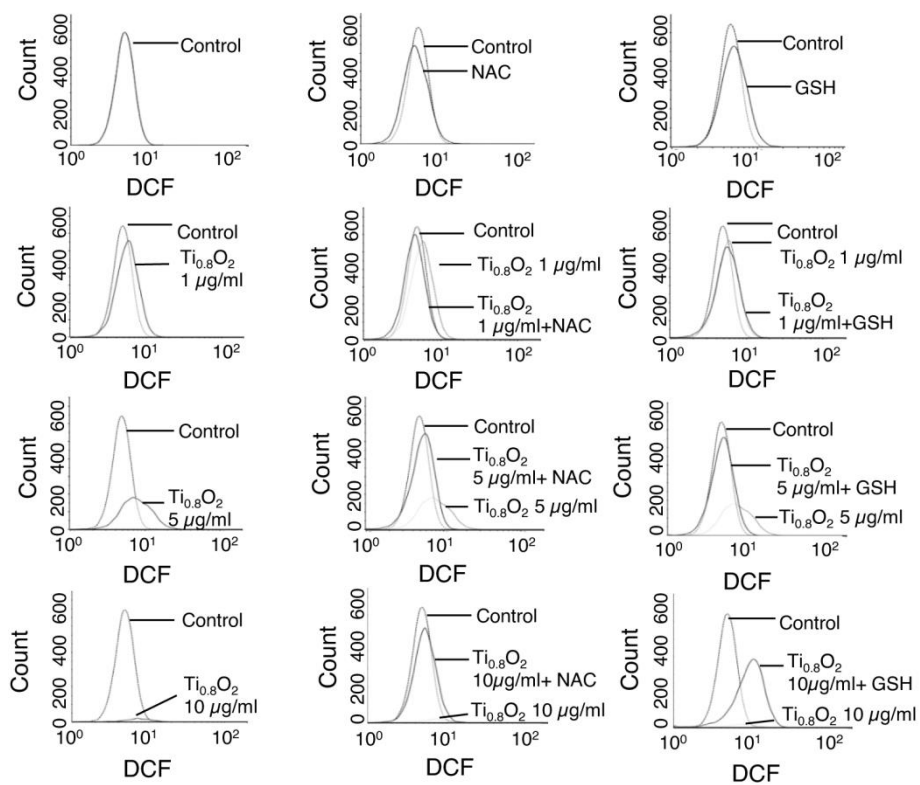
ROS has been considered an important mediator of the initiation and execution of apoptosis and is related to the anti-cancer effect of several drugs (92). We next investigated whether intracellular ROS generation was implicated in the anti-cancer effects of the $Ti_{0.8}O_2$ nanosheets. The intracellular ROS level was evaluated using the fluorescent probe DCFH-DA. The results showed that treatment with $Ti_{0.8}O_2$ nanosheets increased intracellular ROS generation (Figure 17).



H460



A549

Figure 17 The effect of $Ti_{0.8}O_2$ nanosheets on intracellular ROS induction

In order to investigate the protective effect of N-acetylcysteine (NAC) or glutathione (GSH) as a potent antioxidant on $\text{Ti}_{0.8}\text{O}_2$ nanosheet-induced cytotoxicity mediated through ROS generation, the H460 and A549 cell lines were pretreated with NAC or GSH for 1 h previous to treatment with the $\text{Ti}_{0.8}\text{O}_2$ nanosheets. We detected a decrease in the ROS level in all the cell lines treated with NAC and GSH (Figure 17), but the cell viability of the cancer cells could not be reversed by the pretreatment with NAC or GSH (Figure 18 A-B). These results suggest that the $\text{Ti}_{0.8}\text{O}_2$ nanosheets induce cytotoxicity in cancer cell lines but do not do this via the generation of ROS.

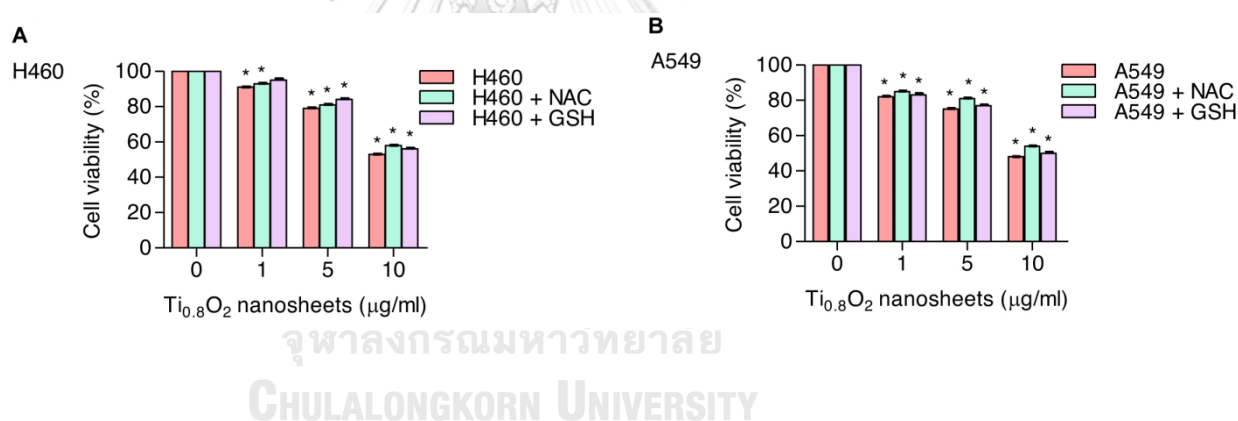


Figure 18 Effect of $\text{Ti}_{0.8}\text{O}_2$ nanosheets on cell viability with the pretreatment of ROS scavenger

Next, we investigated the specific ROS products using a DHE (dihydroethidium) fluorescent probe for the detection of ROS generation and, specifically, the detection of superoxide anions. The results showed that the $\text{Ti}_{0.8}\text{O}_2$ nanosheets had a significant effect on the superoxide anions in H460 cells when they were

treated with $Ti_{0.8}O_2$ nanosheets in a concentration-dependent manner, while the $Ti_{0.8}O_2$ nanosheets had only a slight effect on superoxide anion generation in A549 cells (Figure 19).

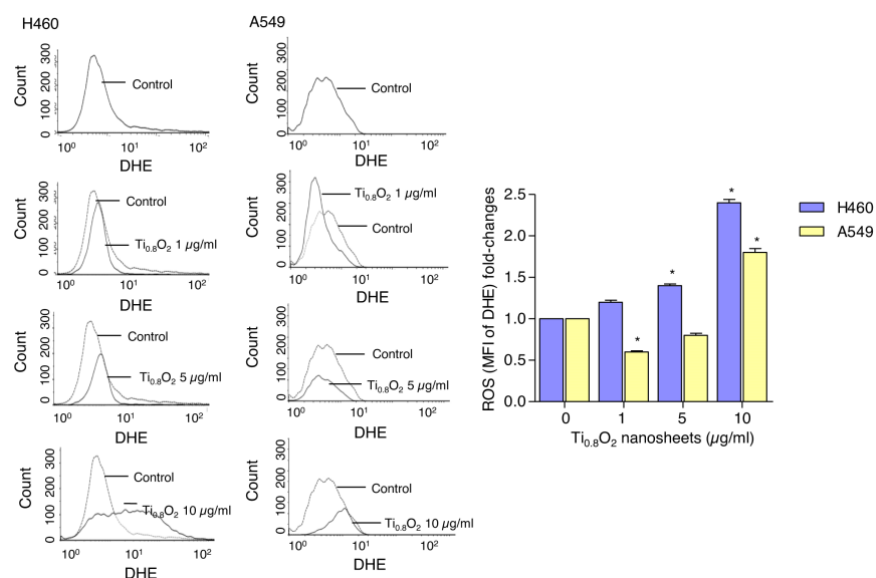


Figure 19 Effect of $Ti_{0.8}O_2$ nanosheets on intracellular superoxide anions induction

In addition, we also investigated the generation of hydroxyl radicals using the HPF (hydroxyphenyl fluorescein) fluorescent probe in both cell lines. The results showed that the $Ti_{0.8}O_2$ nanosheets significantly generated hydroxyl radicals in both cell lines compared with the non-treated cells (Figure 20). According to our obtained data, the pretreatment of cancer cell lines with a potent antioxidant for 1 h could not inhibit H_2O_2 damage, while the $Ti_{0.8}O_2$ nanosheets generated superoxide anion hydroxyl radicals in both cell lines.

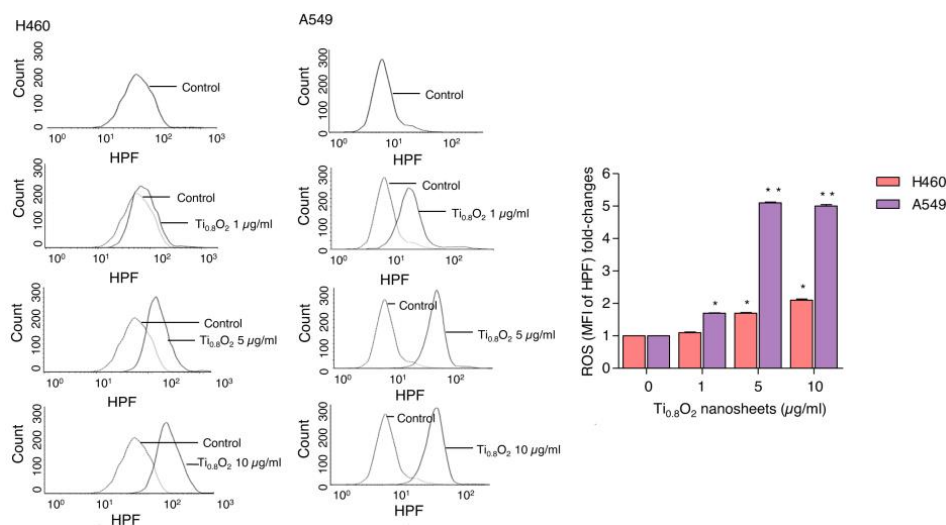


Figure 20 Effect of Ti_{0.8}O₂ nanosheets on intracellular hydroxyl radicals induction

7. Ti_{0.8}O₂ nanosheet-mediated peroxynitrite induces apoptosis in A549 and H460 cells

NO plays a role in apoptosis regulation through its ability to modulate ROS. The cytotoxic action of NO was demonstrated in several systems using diverse cell targets. Interestingly, the cytotoxicity of NO was shown to mediate via the interaction of NO with superoxide to form a highly reactive peroxynitrite (ONOO⁻) (93). Consequently, we analyzed the cellular NO levels in response to the Ti_{0.8}O₂ nanosheets using DAF-FM DA as a fluorescent probe. The NO levels were found to be increased in a concentration-dependent manner (Figure 21 A, C). Additionally, co-treatment with PTIO (a NO scavenger) and/or MnTBAP (a superoxide anion inhibitor) inhibited Ti_{0.8}O₂ nanosheet-induced cell death by increasing cell viability (Figure 21 B, D). The results suggest that Ti_{0.8}O₂ nanosheets induce cytotoxicity in cancer cell lines via the

produced peroxynitrite. All data are shown as the mean \pm SEM ($n = 3$). * $p < 0.05$ compared with the untreated control. # $p < 0.05$ compared with cells treated with $Ti_{0.8}O_2$ only

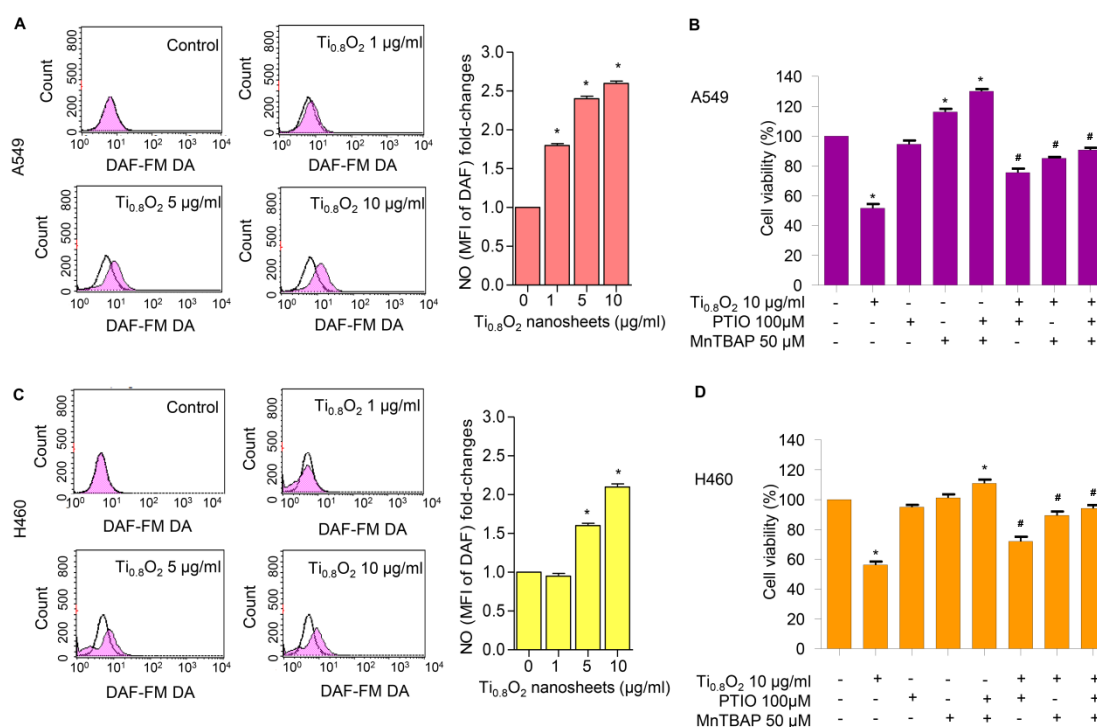


Figure 21 $Ti_{0.8}O_2$ nanosheets induced NO in A549 and H460 cells and mediated peroxynitrite generation

To confirm the previous results, we treated cells with $Ti_{0.8}O_2$ nanosheets and/or pretreated them with PTIO and/or MnTBAP and then determined the cellular NO level by staining with DAF-FM DA and then visualization under a fluorescence microscope. The results showed that the co-treatment with these inhibitors decreased peroxynitrite levels in all the cancer cells (Figure 22).

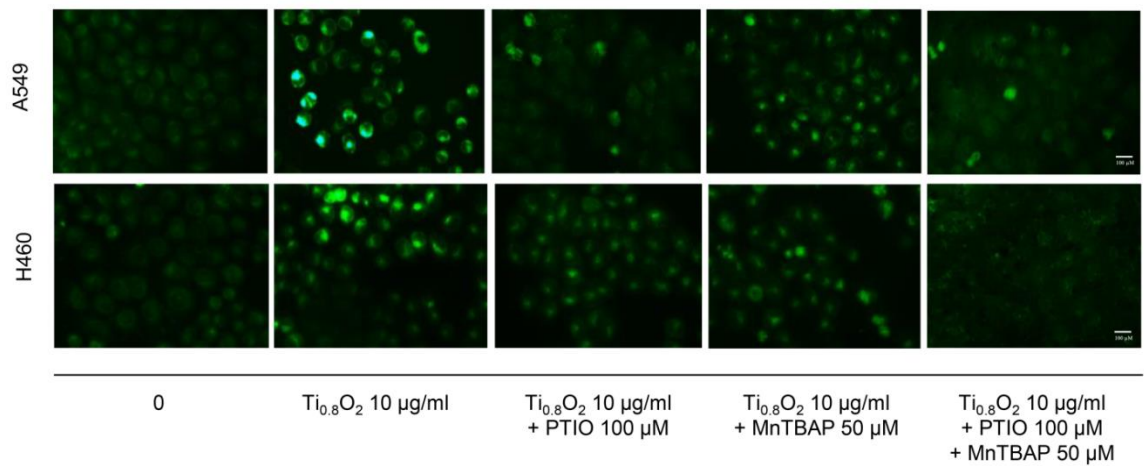


Figure 22 Cellular NO level stained with DAF-FM DA in cells treated with $Ti_{0.8}O_2$ nanosheets

Then, we observed whether increased peroxynitrite was required for cell apoptosis induced by $Ti_{0.8}O_2$ nanosheets. The results showed that the co-treatment with these inhibitors was able to inhibit apoptosis cell death, as shown in Figure 23. Collectively, these results indicated that peroxynitrite generation could play a role in mediating $Ti_{0.8}O_2$ nanosheet-induced cell apoptosis.

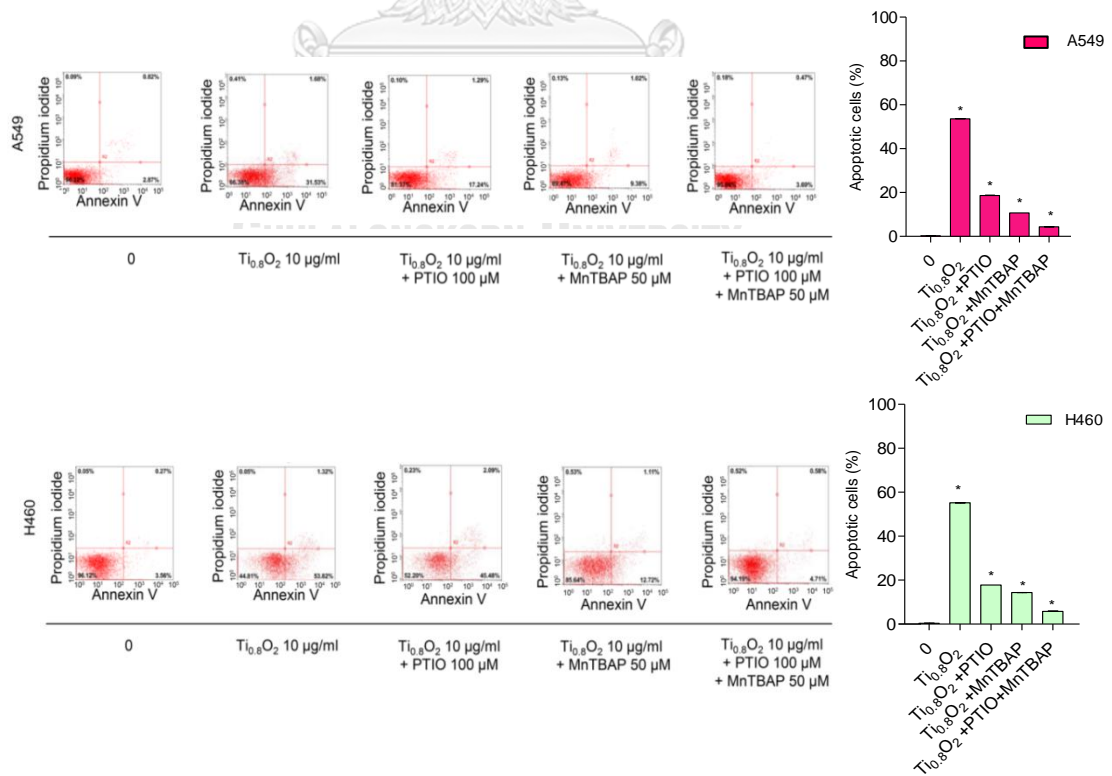


Figure 23 $Ti_{0.8}O_2$ nanosheet-mediated peroxynitrite induces apoptosis
in A549 and H460 cells

8. $Ti_{0.8}O_2$ nanosheet-mediated peroxynitrite induces apoptosis in lung cancer cells via p53 upregulation

Since then, several cell types have been shown to undergo apoptosis in response to NO or peroxynitrite. A previous study reported that peroxynitrite was associated with p53 regulation to induce cancer cell death (94). Therefore, we examined the effect of $Ti_{0.8}O_2$ nanosheets when combined with PTIO and/or MnTBAP. Western blot analysis was performed to evaluate the p53 protein levels after 10 $\mu\text{g/mL}$ $Ti_{0.8}O_2$ nanosheet treatment in all the cell lines. The results showed that the p53 protein levels in all the cell lines were significantly increased with the $Ti_{0.8}O_2$ -nanosheets-alone treatment compared with those of the non-treatment control and another condition treatment (Figure 24). Blots were reprobated with β -actin to confirm the equal loading of samples. The relative protein levels were calculated by densitometry. Data are shown as the mean \pm SEM (n = 3). * $p < 0.05$ versus non-treated control.

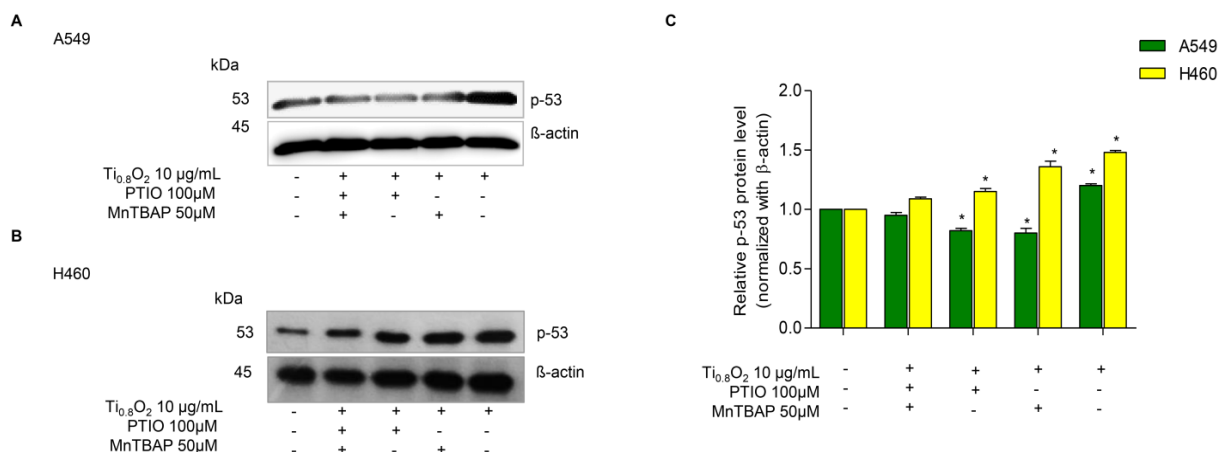


Figure 24 Peroxynitrite-potentiated cell apoptosis through the p53 protein

Taken together, it could be concluded that the Ti_{0.8}O₂ nanosheets induced cancer cell death by the induction of peroxynitrite generation, which activated p53, leading to cancer cell apoptosis. The immunofluorescence staining results supported our finding that Ti_{0.8}O₂ nanosheets, in combination with PTIO and MnTBAP, caused a dramatic decrease in the levels of p53 and P-p53 in both cell lines (Figure 25). These results indicate that the pro-apoptotic effect of Ti_{0.8}O₂ nanosheets for inducing NO is a result of the formation of peroxynitrite, which then induces p53-dependent apoptosis in all the cell lines.

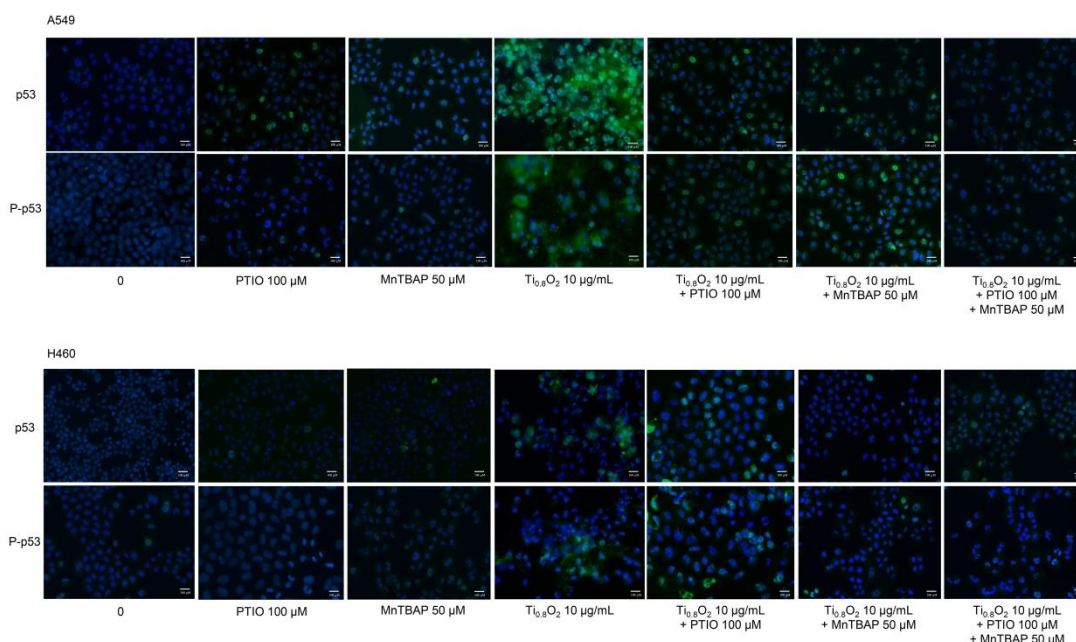


Figure 25 The expressions of p53 and P-p53 were analyzed by immunofluorescence staining in A549 and H460 cells

9. $Ti_{0.8}O_2$ nanosheets increase p53 function but not through p53 proteasomal degradation

In general, p53 functions as a tumor suppressor protein in response to oncogenic stress signals (95). The essential role of p53 is emphasized by the fact that this protein is commonly deregulated or altered in human malignancies (96, 97). The activation of p53 initiates a variety of cellular responses that stop the cell cycle, induce senescence, and activate apoptosis. The key to the regulation of p53 is the control of its stability, which is mainly arranged through a network of ubiquitination reactions. We further evaluated the effect of the $Ti_{0.8}O_2$ nanosheets on p53 protein stability using the cycloheximide (CHX) chasing assay. CHX can inhibit protein biosynthesis and is widely used to investigate the half-life of proteins (98). Therefore, H460 and A549 cells were treated with $Ti_{0.8}O_2$ nanosheets

in the presence or absence of CHX, and the level of p53 over time was determined. Figure 26 show that in the condition where protein production was blocked, the $Ti_{0.8}O_2$ nanosheets increased the stability of the p53 protein. A difference was first detected at 90 min after $Ti_{0.8}O_2$ nanosheet treatment (Figure 26). The relative protein levels are reported ($n = 3$). * $p < 0.05$, ** $p < 0.01$ compared with the untreated control at 0 min, and # $p < 0.05$, ## $p < 0.01$ compared with the untreated control at the same time.

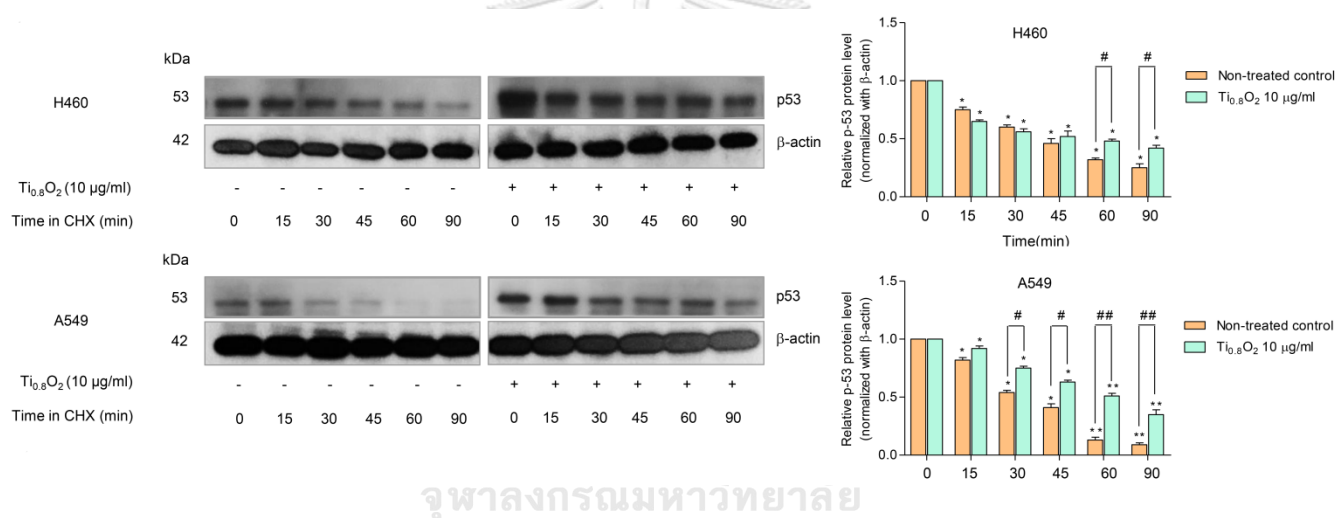


Figure 26 Effect of $Ti_{0.8}O_2$ nanosheets on the half-life of p53

We also determined the p53 protein's half-life and found that the half-life of the p53 protein was approximately 60 min in the $Ti_{0.8}O_2$ nanosheet-treated cells; In contrast, in the non-treated control cells, the half-life was about 30–40 min (Figure 27).

Cell lines	Ti _{0.8} O ₂ (µg/ml)	p53 half-life (min)
H460	0	43.52
	10	58.29
A549	0	31.98
	10	59.87

Figure 27 The half-lives of the p53 protein in the Ti_{0.8}O₂ nanosheet-treated cells

Moreover, the turnover of the p53 protein is tightly regulated by ubiquitin–proteasome degradation. Thus, we used the specific proteasome inhibitor (MG132) to investigate whether the Ti_{0.8}O₂ nanosheets increased p53 stability via the inhibition of proteasomal degradation. Co-immunoprecipitation was also used to test the premise of ubiquitin-mediated p53 degradation in H460 and A549 cells after treatment with 10 µg/mL of Ti_{0.8}O₂ nanosheets and in non-treated control cells for 1 h. Figure 28 shows that the polyubiquitination of p53 was slightly diminished after Ti_{0.8}O₂ nanosheet treatment when compared with control. p53-ubiquitin complexes were quantified by densitometry. The relative protein levels are reported ($n = 3$). * $p < 0.05$, ** $p < 0.01$ compared with the untreated control.

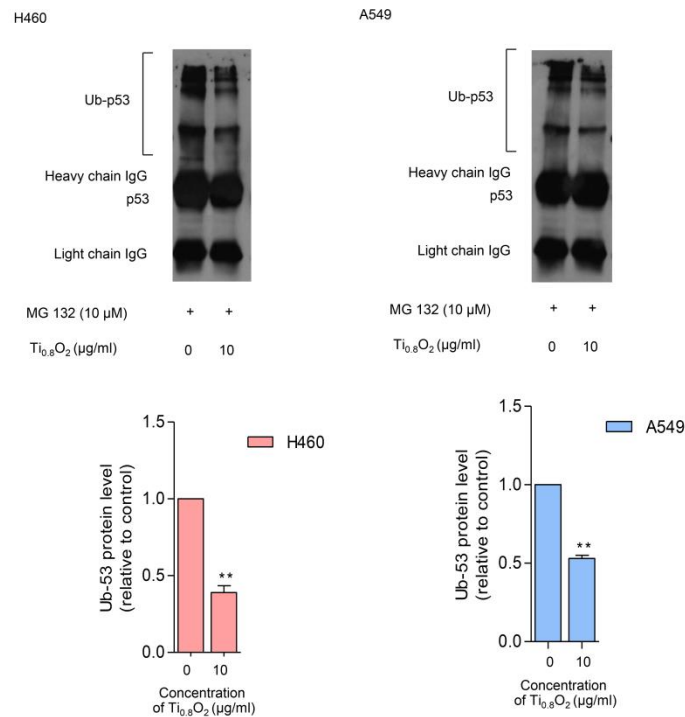


Figure 28 Ti_{0.8}O₂ nanosheet decreases ubiquitin-mediated p53 proteasomal degradation

10. S-nitrosylation in the regulation of stability of the tetrameric p53 protein-protein complex

NO exerts its effects via the formation of S-nitrosylation of cysteine (Cys) residues. S-nitrosylation is a significant post-translational modification that affects p53 functionality (99). S-nitrosylation of a single Cys within HDM2 inhibits p53 binding and thereby stabilizes p53 and activates p53-dependent transcription (100). We tested whether peroxynitrite may directly control p53 by S-nitrosylation and the activation of p53. To evaluate the structural stability of the p53 core domain tetramer without DNA bound (PDB ID: 3KMD) (Figure 29).

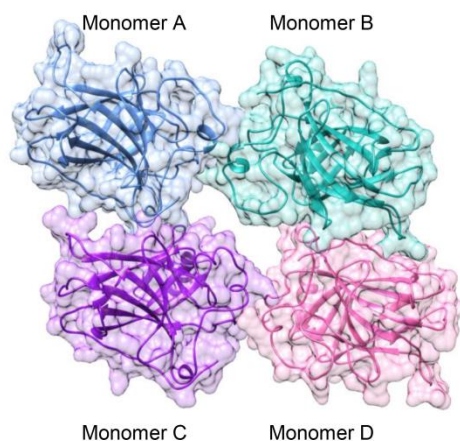


Figure 29 Three-dimensional (3D) structure of the tetrameric p53

The number of intermolecular hydrogen bonds formed between each monomer at the protein-protein interface was monitored along with the simulation time. Note that a hydrogen bond is defined by the following geometric criteria: (i) the distance between the hydrogen bond donor and acceptor atoms is less than 3.5 Å, and (ii) the angle between D-H...A is larger than 120°. The obtained results showed that there was an average of $\sim 10 \pm 2$ hydrogen bonds steadily formed over the course of the simulation time (Figure 30, top). This observation suggested that our simulation model was highly stable. Therefore, 100 equilibrated MD snapshots, extracted from the last 20 ns, were used for further analysis in terms of the $\Delta G_{\text{bind}}^{\text{residue}}$ calculation.

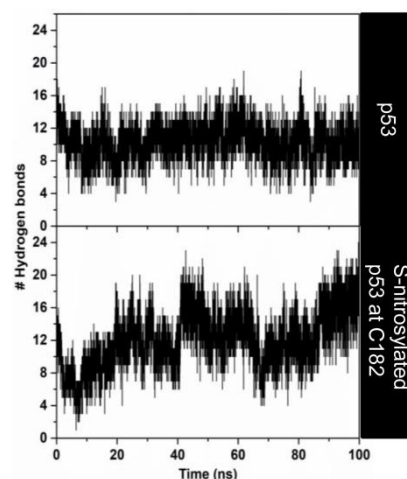


Figure 30 Time evolution of the total number of intermolecular hydrogen bonds formed between each monomer of the p53 core domain and its adjacent monomer

The $\Delta G_{\text{bind}}^{\text{residue}}$ value was then calculated to verify the crucial amino acids involved in protein binding at the interface region of each monomer. The total contributing energy from each amino acid for the protein-protein complex is shown in Figure 31 (top), where the positive and negative $\Delta G_{\text{bind}}^{\text{residue}}$ values are associated with protein destabilization and stabilization, respectively. It is noteworthy that only amino acids exhibiting a $\Delta G_{\text{bind}}^{\text{residue}}$ of < -1.5 kcal/mol were marked as the key binding residues. The results showed that the crucial residues (L93, N167, M169, C176, P177, and E180 for monomer A; H178, E180, R181, N200, L201, and V225 for monomer B; C176, P177, H178, E180, R181, E198, L201, E224, V225, and H233 for monomer C; V97, N100, N167, M169, C176, P177, E180, and R181 for monomer D) played a pivotal role in the tetrameric protein-protein stabilization. Based on this calculation and upon visual inspection, it can be assumed that the cysteine residue within the protein-protein interface, particularly

C182, is most likely to be a critical residue, which would be expected to be related to the S-nitrosylation site and, consequently, would lead to an increase in protein stability.

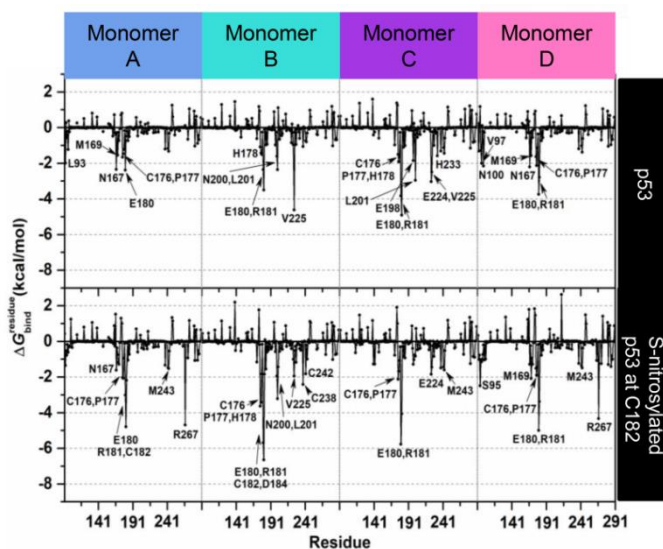


Figure 31 The total contributing energy from each amino acid of the tetrameric p53 protein-protein complex

To clarify such a hypothesis, the influence of S-nitrosylation on the C182 residue of p53 upon its binding interaction with each monomeric p53 was investigated by means of MD simulation, as per the native p53 system. The simulation indicated that the total number of intermolecular hydrogen bonds between four monomeric proteins was slightly increased over the whole simulation, with an average value of $\sim 12 \pm 2$ hydrogen bonds, particularly in the last 10 ns (90–100 ns), in which the number of hydrogen bonds was found to be up to ~ 20 (Figure 30, bottom). This reflected that the S-nitrosylated C182 resulted in higher stability of the tetrameric protein-protein complex compared to the native p53. In addition, the

occurrence of C182 S-nitrosylation appeared to induce the surrounding residues, located in the interface region, to bind more tightly to each other, especially residues 176–186 (Figure 31 (bottom) and Figure 32). Among these amino acids, the lowest $\Delta G_{\text{bind}}^{\text{residue}}$ value (~ -5 to -7 kcal/mol) was observed for residue R181, most likely owing to the indirect stabilizing effect of the S-nitrosylation at C182. This was probably one of the reasons why the S-nitrosylation culminated in the higher stability of p53, as observed in the experimental data.

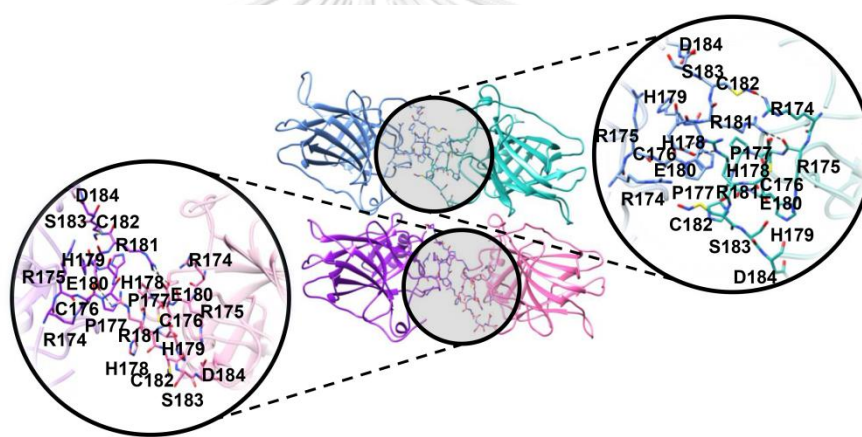


Figure 32 The representative 3D structure taken from the last MD snapshot of the S-nitrosylation system

To confirm the effect of such a nanosheet in the induction of S-nitrosylation in the cells, we further evaluated the induction of S-nitrosylated proteins in response to $\text{Ti}_{0.8}\text{O}_2$ nanosheets. Specific S-nitrosylated protein detection was done using the Pierce S-nitrosylation Western blot kit assay, as described in Materials and Methods. The results revealed that S-nitrosylated proteins were dramatically increased in the $\text{Ti}_{0.8}\text{O}_2$ -treated cells compared with the non-treated control group (Figure 33). S-

nitrosylated proteins determined by Pierce S-nitrosylation Western blot assay. Relative-to-control protein levels are reported ($n = 3$). ** $p < 0.01$ compared with the untreated control at the same time. Taken together, the findings highlight the impact of $Ti_{0.8}O_2$ -induced peroxynitrite in promoting S-nitrosylation and increasing the stability of the tetrameric p53 protein-protein complex, which is responsible for apoptosis cell death in NSCLC.

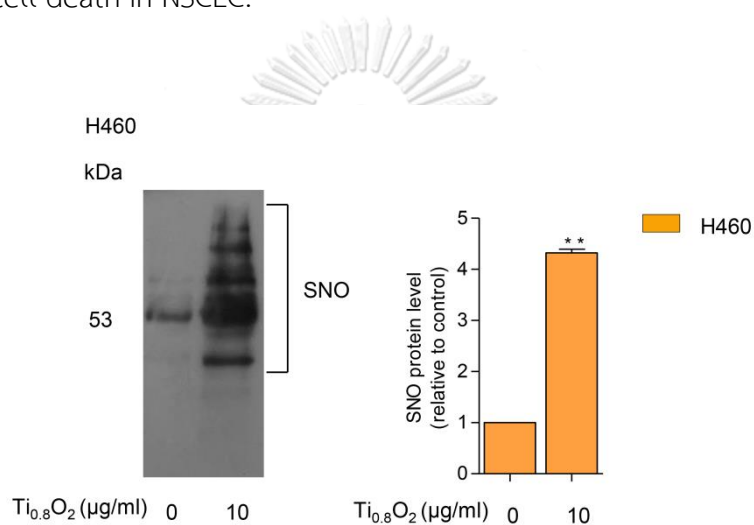


Figure 33 $Ti_{0.8}O_2$ induction of S-nitrosylation in the cells

DISCUSSION

Lung cancer remains the major cause of cancer death worldwide. Nowadays, nanomaterials are showing remarkable potential to aid the diagnosis and treatment of cancer by enabling the more effective targeting of tumors (101). Previous studies have revealed that nanomaterials can selectively sink into solid tumors, whereby they increase the bioavailability and decrease the toxicity of the encapsulated cytotoxic agents (101, 102). $\text{Ti}_{0.8}\text{O}_2$ (an emerging 2D analog of TiO_2) nanosheets can be derived from the potassium zinc titanate precursor $\text{K}_{0.8}\text{Zn}_{0.4}\text{Ti}_{1.6}\text{O}_4$. The planar surface and functional motifs of such 2D inorganic nanosheets can be modified using a surface engineering process involving chemical bonding or physical adsorption (82), which facilitates applications in physiological environments, through, e.g., their biostability improvement, site-specific targeting capability, and multiple theranostic functions to facilitate oncological applications (102-104).

Although TiO_2 nanoparticles and nanotubes have been extensively investigated for their possible applications (104, 105), to the best of our knowledge, there have been limited studies on $\text{Ti}_{0.8}\text{O}_2$ nanosheets. Consequently, here, we show for the first time that $\text{Ti}_{0.8}\text{O}_2$ nanosheets can distinctively induce anti-cancer activity in human non-small cell lung cancer cells and advanced lung cancer cells from patients. This effect was demonstrated in several lung cancer lines in comparison to common chemotherapeutic drugs used in lung cancer

patients. The $\text{Ti}_{0.8}\text{O}_2$ nanosheets significantly increased cancer cell death in a concentration-dependent manner (Figure 8-11). Moreover, the $\text{Ti}_{0.8}\text{O}_2$ nanosheets also mediated apoptosis in lung cancer cells in a concentration-dependent manner (Figure 10-11). Moreover, SEM analysis revealed that 10 $\mu\text{g}/\text{mL}$ $\text{Ti}_{0.8}\text{O}_2$ nanosheets altered cell morphology, while TEM analysis for the characterization of the $\text{Ti}_{0.8}\text{O}_2$ nanosheets in cells showed that the $\text{Ti}_{0.8}\text{O}_2$ nanosheets could appropriately disperse into H460 cells more easily than in DP cells (Figure 13). A previous study showed that various types of nanoparticles (NPs), such as copper oxide nanoparticles, could be used to induce anti-cancer activity in cancer cells (106). Next, we further examined whether the $\text{Ti}_{0.8}\text{O}_2$ nanosheets could induce cell apoptosis in H460 and A549 cells. We found that the treatment of lung cancer cells with $\text{Ti}_{0.8}\text{O}_2$ nanosheets resulted in a significant induction of p53, which may, at least in part, play a role in $\text{Ti}_{0.8}\text{O}_2$ nanosheet-mediated apoptosis (Figure 14). Consistent with our findings, a previous study showed that FePt/GO nanosheets suppressed proliferation and induced apoptosis in H1975 cells, and silver nanoparticles induced apoptosis in human colon cancer cells mediated by p53 (107, 108).

Most cancers possess aberrant or disrupted p53 pathways. Intervention to restore or enhance p53 activity is a promising cancer treatment strategy (109). Interestingly, in this study, we further confirmed that $\text{Ti}_{0.8}\text{O}_2$ nanosheets also had cytotoxicity in patient-derived primary lung cancer cells, with a lower IC_{50}

compared to some other first-line chemotherapeutic drugs tested (Figure 15-16). In addition, we have provided supportive information explaining that the cancer cell selectivity of $Ti_{0.8}O_2$ nanosheets may be caused by the generation of superoxide anions, similar to findings in a previous study (110). Another previous study suggested that the effect of nanosilver on apoptosis was via ROS generation and the JNK-dependent pathway (111). In addition, aminoflavone (AF) has been demonstrated to cause selective cell death induction in breast cancer cells, with minimal toxicity to normal breast cells. Aminoflavone caused an ROS increase, which is linked with the activation of caspase 3 and apoptosis, which can be prevented by the pretreatment of the cells with N-acetyl-L-cysteine (NAC) (112, 113). However, the generation of ROS was not associated with lung cancer cell death when the cells were pretreated with NAC or GSH, and the cell viability of the cancer cells could not be reversed (Figure 18). This result suggests that the $Ti_{0.8}O_2$ nanosheets may generate other ROS for inducing cell death. In addition, we investigated the superoxide anion level in lung cancer cells because superoxide is primary oxygen radical that is produced when an oxygen molecule receives one electron. The results showed that the superoxide anion levels were increased in a concentration-dependent manner in H460 cells, while $Ti_{0.8}O_2$ had decreased superoxide anion in concentrations between 1 and 5 g/mL and then increased in concentration to 10 g/mL in A549 cells. Consistent with previous studies showed that FACS analysis also revealed a significant time dependent increase in the

percentage of cells positive for DHE indicating the potential of grape seed extract (GSE) to superoxide in most of the NSCLC cells. In A549 cells, GSE treatment caused a robust increase superoxide within 30 min, which slowly declined thereafter. But in H460 cells, GSE treatment caused a robust increase superoxide within 3 h, which slowly declined thereafter (114). Consequently, in this study we treated cells with $Ti_{0.8}O_2$ for 3 h could be associated with increase superoxide generation in H460 cells in time dependent. However, $Ti_{0.8}O_2$ treatment of A549 cells for 3 h was associated with decreased superoxide generation at low concentrations of $Ti_{0.8}O_2$, but increased superoxide generation at high concentrations of $Ti_{0.8}O_2$. It may be that at low concentrations, the superoxide is lost, but at higher concentration, more superoxide can be measured. Altogether, the different time in superoxide generation depend on cellular bioprocess of each cells type. Therefore, we investigated the NO level in lung cancer cells because its activity could be associated with cell death, as previously described (115). The results showed that the NO levels were increased in a concentration-dependent manner (Figure 22). Additionally, co-treatment of $Ti_{0.8}O_2$ nanosheets with PTIO (NO scavenger) or MnTBAP (superoxide anion inhibitor) inhibited $Ti_{0.8}O_2$ nanosheet-induced cell death by increasing cell viability. Much evidence has demonstrated that the direct toxicity of NO is modest but can be greatly enhanced by reacting with the superoxide anion to form peroxynitrite ($ONOO^-$), which can directly damage DNA and attenuate DNA repair (116, 117). This previous study has shown

that MnTBAP selectively scavenges peroxynitrite from a superoxide-dependent pathway (118, 119). In this study, we used PTIO for blocked NO generation and co-treated with MnTBAP for blocked peroxynitrite from a superoxide-dependent pathway.

p53 is a tumor suppressor gene, regulating apoptosis and cell cycle arrest in cells that have damaged DNA. We found that the generation of peroxynitrite after treatment with $Ti_{0.8}O_2$ nanosheets upregulated the expression of p53-mediated apoptosis (Figure 23-24). The data support the hypothesis that peroxynitrite contributes to the tumorigenic properties of p53 mutations. Peroxynitrite was found to induce mitochondrial permeability transition changes and promote apoptosis in cell-free systems containing mitochondria (52). In many cancer types, the *TP53* gene is often mutated or deleted, which inactivates the tumour suppression activity of the p53 protein. However, loss of p53 tumour-suppressor activity can also occur through amplification of MDM2. As MDM2 is a negative regulator of p53, this promotes p53 degradation and inhibits p53 tumour suppressor activity (120). The degradation of p53 in normal cells is regulated through ubiquitination by the E3 ubiquitin ligase Mdm2 (121). Furthermore, overexpression of MDM2 has been linked to worse prognosis in different types of tumors, correlating with altered p53 protein levels, although it has not been confirmed whether these tumors have wild-type or mutant p53 (122). In addition to small molecules have also been identified to disrupt MDM2-p53 interaction,

resulting in accumulation of p53 and its anti-tumor activity (123). In this study, we found that under $Ti_{0.8}O_2$ nanosheet treatment, the half-life of p53 was dramatically increased. The cycloheximide-based assay showed that the half-life of p53 in response to 10 $\mu\text{g/mL}$ $Ti_{0.8}O_2$ nanosheets was about 60 min in comparison to 30–40 min in non-treated control cells (Figure 26-27). After applying the selective proteasome inhibitor (MG132), we monitored the levels of the p53-ubiquitin complex and found that the formation of the complex was dramatically decreased in the $Ti_{0.8}O_2$ nanosheet-treated cancer cells (Figure 28). Thus confirming that the $Ti_{0.8}O_2$ nanosheets-mediated p53 activity did not occur through ubiquitin–proteasome degradation. Here, we have revealed novel information regarding the role of reactive nitrogen species, especially peroxynitrite, in the regulation of p53 tetramerization. Our results showed that when the cells were exposed to the nanosheets, the intracellular level of peroxynitrite was highly upregulated (Figure 19-22). Concomitantly, increased p53 was detected (Figure 24) with the decrease in the p53-ubiquitin complex (Figure 28), implying that the upregulation of p53 occurs as a result of preventing its degradation process.

Peroxyntirite is considered an important biological inducer via its direct interaction with protein in S-nitrosylation. S-nitrosylation is a rapid interaction wherein NO is attached to a thiol moiety of the target protein, forming S-NO at the cysteine amino acid (124). More than 1000 proteins have been found as the

targets of *S*-nitrosylation (125), and it was noted that such protein modification resulted in a profound alteration of protein–protein interaction, protein function, protein localization, and protein stability (126). Cellular stress, such as through cisplatin (CDDP) treatment, activates and stabilizes p53 via phosphorylation at the sites of Ser 15 and/or Ser 20, subsequently blocking p53–Mdm2 interaction and suppressing p53 degradation (127).

The p53 protein plays a crucial role as a transcription factor regulating the expression of many proteins controlling cell arrest and apoptosis (128). The p53 protein contains a tetramerization domain (p53TD) and a DNA-binding domain (p53DBD) which are important for protein functions (129). Interestingly, evidence indicates that the activity of the p53 protein is highly dependent on tetrameric complex formation and complex stability (130). Therefore, molecules capable of stabilizing the tetrameric form of the proteins could be promising therapeutic tools. Furthermore, we report additional studies on the role of hydrogen bond interactions in protein stability and the key binding residues of p53 to direct the effect of *S*-nitrosylation (Figure 29-33). In globular proteins, there are intermolecular hydrogen bonds between the protein and water molecules and between water molecules that are bound with the proteins (131). Here, we used computational tools to predict the point of *S*-nitrosylation on the p53 protein and found that peroxynitrite may directly control p53 by *S*-nitrosylation to stabilize the tetrameric structure of this protein. To estimate the contribution of these

hydrogen bonds to the conformational stability of a protein compared with that of the native p53 and *S*-nitrosylation of p53 (132), we investigated the relationship between *S*-nitrosylation and the increase in p53 stability. We identified the H-bond intermolecular interactions between a monomer of native p53 compared to its *S*-nitrosylation form and found higher stability of the tetrameric protein–protein complex in comparison to the native p53, especially regarding the reactivity of the cysteine at residue 182 in p53. The high reactivity of specific cysteine thiol groups in p53 is likely important for the regulation of p53 and its degradation pathways (100). Moreover, peroxy nitrite has been shown to activate the opening of mitochondrial pores that release cytochrome c into the cytoplasm (133). According to our results, we found that peroxy nitrite induces p53 stability and increases the activation of Bax and, subsequently, caspase 3. These changes are all hallmarks of cell death (Figure 34). Furthermore, the nanosheets were shown to generate peroxy nitrite in aggressively driven mechanisms, including the process for the *S*-nitrosylation of p53 for protein stabilization. This novel finding on the role of $\text{Ti}_{0.8}\text{O}_2$ nanosheets in p53-mediated apoptosis may have important implications in cancer treatment.

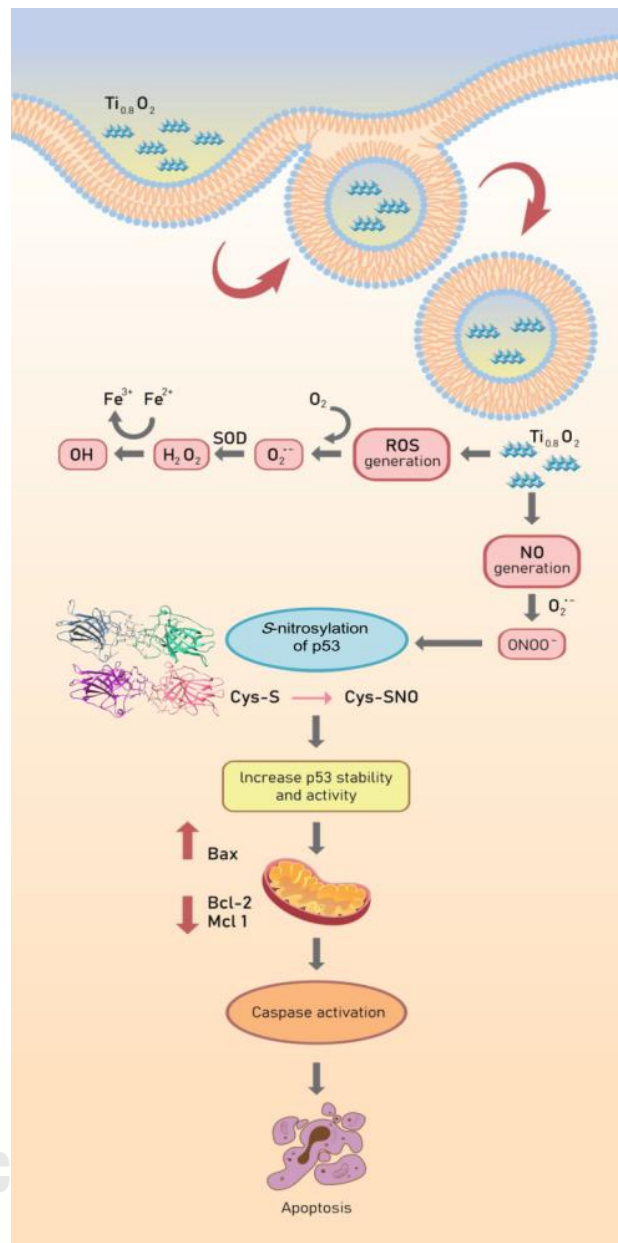
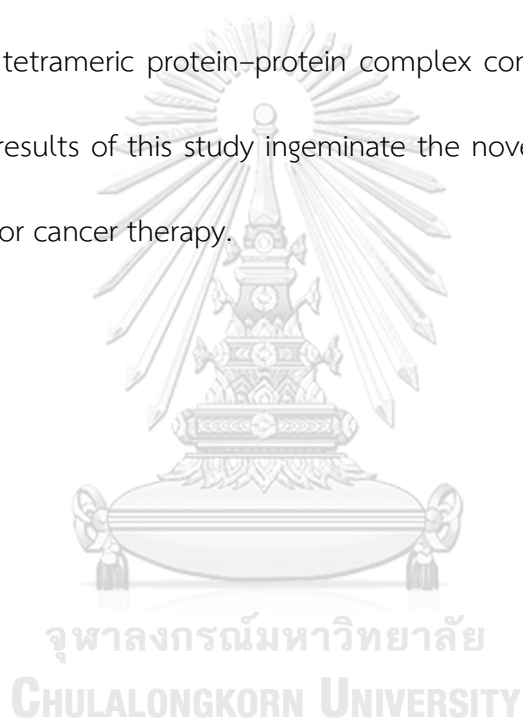


Figure 34 Schematic diagram of $\text{Ti}_{0.8}\text{O}_2$ nanosheet-mediated peroxynitrite generation that was associated with apoptosis via p53 upregulation in non-small cell lung cancer

CONCLUSIONS

In conclusion, our present study, for the first time, provides information on the effect of $\text{Ti}_{0.8}\text{O}_2$ nanosheet-induced apoptosis through a molecular mechanism involving peroxynitrite generation. After treatment with $\text{Ti}_{0.8}\text{O}_2$ nanosheets, it may directly control p53 by S-nitrosylation to stabilize the tetrameric structure of this protein. This reflects that the S-nitrosylation at C182 of p53 results in higher stability of the tetrameric protein-protein complex compared to the native p53. Therefore, the results of this study ingeminate the novel mechanism of action of nanomaterials for cancer therapy.



REFERENCES



จุฬาลงกรณ์มหาวิทยาลัย
CHULALONGKORN UNIVERSITY

1. Herbst RS, Morgensztern D, Boshoff C. The biology and management of non-small cell lung cancer. *Nature*. 2018;553(7689):446-54.
2. Chen J. The Cell-Cycle Arrest and Apoptotic Functions of p53 in Tumor Initiation and Progression. *Cold Spring Harb Perspect Med*. 2016;6(3):a026104-a.
3. Dai C, Gu W. p53 post-translational modification: deregulated in tumorigenesis. *Trends Mol Med*. 2010;16(11):528-36.
4. Meek DW, Anderson CW. Posttranslational modification of p53: cooperative integrators of function. *Cold Spring Harb Perspect Biol*. 2009;1(6):a000950-a.
5. Zhang J, Huang K, O'Neill KL, Pang X, Luo X. Bax/Bak activation in the absence of Bid, Bim, Puma, and p53. *Cell Death & Disease*. 2016;7(6):e2266-e.
6. Tang D, Kang R, Berghe TV, Vandenabeele P, Kroemer G. The molecular machinery of regulated cell death. *Cell Research*. 2019;29(5):347-64.
7. Chène P. The role of tetramerization in p53 function. *Oncogene*. 2001;20(21):2611-7.
8. Hainaut P, Milner J. Redox modulation of p53 conformation and sequence-specific DNA binding in vitro. *Cancer Res*. 1993;53(19):4469-73.
9. Buzek J, Latonen L, Kurki S, Peltonen K, Laiho M. Redox state of tumor suppressor p53 regulates its sequence-specific DNA binding in DNA-damaged cells by cysteine 277. *Nucleic Acids Res*. 2002;30(11):2340-8.
10. Scotcher J, Clarke DJ, Mackay CL, Hupp T, Sadler PJ, Langridge-Smith PRR. Redox regulation of tumour suppressor protein p53: identification of the sites of

hydrogen peroxide oxidation and glutathionylation. *Chemical Science*. 2013;4(3):1257-69.

11. Kim DH, Kundu JK, Surh YJ. Redox modulation of p53: mechanisms and functional significance. *Mol Carcinog*. 2011;50(4):222-34.

12. Maillet A, Pervaiz S. Redox Regulation of p53, Redox Effectors Regulated by p53: A Subtle Balance. *Antioxidants & Redox Signaling*. 2011;16(11):1285-94.

13. Lehnert BE. Nitric Oxide and Nitrogen Dioxide Toxicology. In: Corn M, editor. *Handbook of Hazardous Materials*. Boston: Academic Press; 1993. p. 475-89.

14. Mengel A, Chaki M, Shekariesfahlan A, Lindermayr C. Effect of nitric oxide on gene transcription – S-nitrosylation of nuclear proteins. *Frontiers in Plant Science*. 2013;4(293).

15. Weinberger B, Laskin DL, Heck DE, Laskin JD. The Toxicology of Inhaled Nitric Oxide. *Toxicological Sciences*. 2001;59(1):5-16.

16. Hess DT, Matsumoto A, Kim S-O, Marshall HE, Stamler JS. Protein S-nitrosylation: purview and parameters. *Nature Reviews Molecular Cell Biology*. 2005;6(2):150-66.

17. Radi R. Oxygen radicals, nitric oxide, and peroxynitrite: Redox pathways in molecular medicine. *Proceedings of the National Academy of Sciences*. 2018;115(23):5839.

18. Pacher P, Beckman JS, Liudet L. Nitric oxide and peroxynitrite in health and disease. *Physiol Rev*. 2007;87(1):315-424.

19. Boulaiz H, Alvarez PJ, Ramirez A, Marchal JA, Prados J, Rodríguez-Serrano F, et al. Nanomedicine: application areas and development prospects. *International journal of molecular sciences*. 2011;12(5):3303-21.
20. Zhang W, Yu J, Chang H. Two dimensional nanosheets as conductive, flexible elements in biomaterials. *Journal of Materials Chemistry B*. 2015;3(25):4959-64.
21. Petpiroon N, Bhummaphan N, Soonnarong R, Chantarawong W, Maluangnont T, Pongrakhananon V, et al. TiO₂ Nanosheets Inhibit Lung Cancer Stem Cells by Inducing Production of Superoxide Anion. *Molecular Pharmacology*. 2019;mol.118.114447.
22. Bray F, Ferlay J, Soerjomataram I, Siegel RL, Torre LA, Jemal A. Global cancer statistics 2018: GLOBOCAN estimates of incidence and mortality worldwide for 36 cancers in 185 countries. *CA Cancer J Clin*. 2018;68(6):394-424.
23. Virani S, Bilheem S, Chansaard W, Chitapanarux I, Daoprasert K, Khuanchana S, et al. National and Subnational Population-Based Incidence of Cancer in Thailand: Assessing Cancers with the Highest Burdens. *Cancers*. 2017;9(8):108.
24. Zappa C, Mousa SA. Non-small cell lung cancer: current treatment and future advances. *Transl Lung Cancer Res*. 2016;5(3):288-300.
25. Molina JR, Yang P, Cassivi SD, Schild SE, Adjei AA. Non-small cell lung cancer: epidemiology, risk factors, treatment, and survivorship. *Mayo Clin Proc*. 2008;83(5):584-94.

26. Blandin Knight S, Crosbie PA, Balata H, Chudziak J, Hussell T, Dive C. Progress and prospects of early detection in lung cancer. *Open Biol.* 2017;7(9).
27. Hassan M, Watari H, AbuAlmaaty A, Ohba Y, Sakuragi N. Apoptosis and molecular targeting therapy in cancer. *Biomed Res Int.* 2014;2014:150845.
28. Detterbeck FC, Boffa DJ, Kim AW, Tanoue LT. The Eighth Edition Lung Cancer Stage Classification. *Chest.* 2017;151(1):193-203.
29. Detterbeck FC, Postmus PE, Tanoue LT. The Stage Classification of Lung Cancer: Diagnosis and Management of Lung Cancer, 3rd ed: American College of Chest Physicians Evidence-Based Clinical Practice Guidelines. *Chest.* 2013;143(5, Supplement):e191S-e210S.
30. Jones GS, Baldwin DR. Recent advances in the management of lung cancer. *Clin Med (Lond).* 2018;18(Suppl 2):s41-s6.
31. Zappa C, Mousa SA. Non-small cell lung cancer: current treatment and future advances. *Translational Lung Cancer Research.* 2016;5(3):288-300.
32. Majeed U, Manochakian R, Zhao Y, Lou Y. Targeted therapy in advanced non-small cell lung cancer: current advances and future trends. *Journal of Hematology & Oncology.* 2021;14(1):108.
33. Baig S, Seevasant I, Mohamad J, Mukheem A, Huri HZ, Kamarul T. Potential of apoptotic pathway-targeted cancer therapeutic research: Where do we stand? *Cell Death Dis.* 2016;7:e2058.

34. Elmore S. Apoptosis: a review of programmed cell death. *Toxicol Pathol.* 2007;35(4):495-516.
35. Goldar S, Khaniani MS, Derakhshan SM, Baradaran B. Molecular mechanisms of apoptosis and roles in cancer development and treatment. *Asian Pac J Cancer Prev.* 2015;16(6):2129-44.
36. Guicciardi ME, Gores GJ. Life and death by death receptors. *Faseb j.* 2009;23(6):1625-37.
37. Vousden KH, Lane DP. p53 in health and disease. *Nat Rev Mol Cell Biol.* 2007;8(4):275-83.
38. Adams JM, Cory S. The Bcl-2 apoptotic switch in cancer development and therapy. *Oncogene.* 2007;26(9):1324-37.
39. Kroemer G, Martin SJ. Caspase-independent cell death. *Nat Med.* 2005;11(7):725-30.
40. Aubrey BJ, Kelly GL, Janic A, Herold MJ, Strasser A. How does p53 induce apoptosis and how does this relate to p53-mediated tumour suppression? *Cell Death Differ.* 2018;25(1):104-13.
41. Melino G, De Laurenzi V, Vousden KH. p73: Friend or foe in tumorigenesis. *Nat Rev Cancer.* 2002;2(8):605-15.
42. Vousden KH, Lu X. Live or let die: the cell's response to p53. *Nat Rev Cancer.* 2002;2(8):594-604.

43. Li P, Nijhawan D, Budihardjo I, Srinivasula SM, Ahmad M, Alnemri ES, et al. Cytochrome c and dATP-dependent formation of Apaf-1/caspase-9 complex initiates an apoptotic protease cascade. *Cell*. 1997;91(4):479-89.
44. Balagurumoorthy P, Sakamoto H, Lewis MS, Zambrano N, Clore GM, Gronenborn AM, et al. Four p53 DNA-binding domain peptides bind natural p53-response elements and bend the DNA. *Proceedings of the National Academy of Sciences of the United States of America*. 1995;92(19):8591-5.
45. Kamada R, Toguchi Y, Nomura T, Imagawa T, Sakaguchi K. Tetramer formation of tumor suppressor protein p53: Structure, function, and applications. *Biopolymers*. 2016;106(4):598-612.
46. Lang V, Pallara C, Zabala A, Lobato-Gil S, Lopitz-Otsoa F, Farrás R, et al. Tetramerization-defects of p53 result in aberrant ubiquitylation and transcriptional activity. *Molecular Oncology*. 2014;8(5):1026-42.
47. D'Abramo M, Bešker N, Desideri A, Levine AJ, Melino G, Chillemi G. The p53 tetramer shows an induced-fit interaction of the C-terminal domain with the DNA-binding domain. *Oncogene*. 2016;35(25):3272-81.
48. Nita M, Grzybowski A. The Role of the Reactive Oxygen Species and Oxidative Stress in the Pathomechanism of the Age-Related Ocular Diseases and Other Pathologies of the Anterior and Posterior Eye Segments in Adults. *Oxid Med Cell Longev*. 2016;2016:3164734.

49. Murphy MP. How mitochondria produce reactive oxygen species. *Biochem J*. 2009;417(1):1-13.
50. Wang Y, Branicky R, Noë A, Hekimi S. Superoxide dismutases: Dual roles in controlling ROS damage and regulating ROS signaling. *J Cell Biol*. 2018;217(6):1915-28.
51. Lü JM, Lin PH, Yao Q, Chen C. Chemical and molecular mechanisms of antioxidants: experimental approaches and model systems. *J Cell Mol Med*. 2010;14(4):840-60.
52. Pryor WA, Squadrito GL. The chemistry of peroxynitrite: a product from the reaction of nitric oxide with superoxide. *Am J Physiol*. 1995;268(5 Pt 1):L699-722.
53. Redza-Dutordoir M, Averill-Bates DA. Activation of apoptosis signalling pathways by reactive oxygen species. *Biochimica et Biophysica Acta (BBA) - Molecular Cell Research*. 2016;1863(12):2977-92.
54. Pflaum J, Schlosser S, Müller M. p53 Family and Cellular Stress Responses in Cancer. *Front Oncol*. 2014;4:285.
55. Vaseva AV, Moll UM. The mitochondrial p53 pathway. *Biochim Biophys Acta*. 2009;1787(5):414-20.
56. Korhonen R, Lahti A, Kankaanranta H, Moilanen E. Nitric Oxide Production and Signaling in Inflammation. *Current drug targets Inflammation and allergy*. 2005;4:471-9.
57. Kim PK, Zamora R, Petrosko P, Billiar TR. The regulatory role of nitric oxide in apoptosis. *Int Immunopharmacol*. 2001;1(8):1421-41.

58. Snyder CM, Shroff EH, Liu J, Chandel NS. Nitric oxide induces cell death by regulating anti-apoptotic BCL-2 family members. *PLoS One*. 2009;4(9):e7059.
59. Packer M, Murphy M. Peroxynitrite Formed by Simultaneous Nitric Oxide and Superoxide Generation Causes Cyclosporin-A-Sensitive Mitochondrial Calcium Efflux and Depolarisation. *European journal of biochemistry / FEBS*. 1995;234:231-9.
60. Kohlgrüber S, Upadhye A, Dybala-Rukes N, McNamara CA, Altschmied J. Regulation of Transcription Factors by Reactive Oxygen Species and Nitric Oxide in Vascular Physiology and Pathology. *Antioxidants & redox signaling*. 2017;26(13):679-99.
61. Trachootham D, Lu W, Ogasawara MA, Nilsa R-DV, Huang P. Redox regulation of cell survival. *Antioxidants & redox signaling*. 2008;10(8):1343-74.
62. Shi D, Gu W. Dual Roles of MDM2 in the Regulation of p53: Ubiquitination Dependent and Ubiquitination Independent Mechanisms of MDM2 Repression of p53 Activity. *Genes & cancer*. 2012;3(3-4):240-8.
63. Fischer NW, Prodeus A, Malkin D, Gariépy J. p53 oligomerization status modulates cell fate decisions between growth, arrest and apoptosis. *Cell Cycle*. 2016;15(23):3210-9.
64. Hafner A, Bulyk ML, Jambhekar A, Lahav G. The multiple mechanisms that regulate p53 activity and cell fate. *Nature Reviews Molecular Cell Biology*. 2019;20(4):199-210.

65. Holley AK, St Clair DK. Watching the watcher: regulation of p53 by mitochondria. *Future Oncol.* 2009;5(1):117-30.
66. Zorov DB, Juhaszova M, Sollott SJ. Mitochondrial reactive oxygen species (ROS) and ROS-induced ROS release. *Physiological reviews.* 2014;94(3):909-50.
67. Jeevanandam J, Barhoum A, Chan YS, Dufresne A, Danquah MK. Review on nanoparticles and nanostructured materials: history, sources, toxicity and regulations. *Beilstein J Nanotechnol.* 2018;9:1050-74.
68. Carriere M, Sauvaigo S, Douki T, Ravanat J-L. Impact of nanoparticles on DNA repair processes: current knowledge and working hypotheses. *Mutagenesis.* 2016;32(1):203-13.
69. Abdal Dayem A, Hossain M, Lee SB, Kim K, Saha S, Yang G-M, et al. The Role of Reactive Oxygen Species (ROS) in the Biological Activities of Metallic Nanoparticles. *International Journal of Molecular Sciences.* 2017;18:120.
70. Fu PP, Xia Q, Hwang H-M, Ray PC, Yu H. Mechanisms of nanotoxicity: Generation of reactive oxygen species. *Journal of Food and Drug Analysis.* 2014;22(1):64-75.
71. Ahamed M, Khan M, Akhtar M, Alhadlaq H, Alshamsan A. Role of Zn doping in oxidative stress mediated cytotoxicity of TiO₂ nanoparticles in human breast cancer MCF-7 cells. *Scientific Reports.* 2016;6:30196.

72. Bai DP, Zhang XF, Zhang GL, Huang YF, Gurunathan S. Zinc oxide nanoparticles induce apoptosis and autophagy in human ovarian cancer cells. *Int J Nanomedicine*. 2017;12:6521-35.
73. Siddiqui MA, Alhadlaq HA, Ahmad J, Al-Khedhairy AA, Musarrat J, Ahamed M. Copper oxide nanoparticles induced mitochondria mediated apoptosis in human hepatocarcinoma cells. *PLoS One*. 2013;8(8):e69534.
74. Cho WS, Kang BC, Lee JK, Jeong J, Che JH, Seok SH. Comparative absorption, distribution, and excretion of titanium dioxide and zinc oxide nanoparticles after repeated oral administration. *Part Fibre Toxicol*. 2013;10:9.
75. Wang L, Sasaki T. Titanium Oxide Nanosheets: Graphene Analogues with Versatile Functionalities. *Chemical reviews*. 2014;114.
76. Maluangnont T, Matsuba K, Geng F, Ma R, Yamauchi Y, Sasaki T. Osmotic Swelling of Layered Compounds as a Route to Producing High-Quality Two-Dimensional Materials. A Comparative Study of Tetramethylammonium versus Tetrabutylammonium Cation in a Lepidocrocite-type Titanate. *Chemistry of Materials*. 2013;25:3137.
77. Yang B, Chen Y, Shi J. Material Chemistry of Two-Dimensional Inorganic Nanosheets in Cancer Theranostics. *Chem*. 2018;4(6):1284-313.
78. Ali ES, Sharker SM, Islam MT, Khan IN, Shaw S, Rahman MA, et al. Targeting cancer cells with nanotherapeutics and nanodiagnostics: Current status and future perspectives. *Seminars in Cancer Biology*. 2021;69:52-68.

79. Lugano R, Ramachandran M, Dimberg A. Tumor angiogenesis: causes, consequences, challenges and opportunities. *Cell Mol Life Sci.* 2020;77(9):1745-70.
80. Cheng Z, Li M, Dey R, Chen Y. Nanomaterials for cancer therapy: current progress and perspectives. *Journal of Hematology & Oncology.* 2021;14(1):85.
81. Sriphan S, Charoonsuk T, Maluangnont T, Vittayakorn N. High-Performance Hybridized Compositized-Based Piezoelectric and Triboelectric Nanogenerators Based on BaTiO₃/PDMS Composite Film Modified with Ti_{0.8}O₂ Nanosheets and Silver Nanopowders Cofillers. *ACS Applied Energy Materials.* 2019;2(5):3840-50.
82. Cho Y, Gorina S, Jeffrey PD, Pavletich NP. Crystal structure of a p53 tumor suppressor-DNA complex: understanding tumorigenic mutations. *Science.* 1994;265(5170):346-55.
83. Anandakrishnan R, Aguilar B, Onufriev AV. H++ 3.0: automating pK prediction and the preparation of biomolecular structures for atomistic molecular modeling and simulations. *Nucleic Acids Res.* 2012;40(W1):W537-W41.
84. Nutho B, Rungrotmongkol T. Binding recognition of substrates in NS2B/NS3 serine protease of Zika virus revealed by molecular dynamics simulations. *J Mol Graph Model.* 2019;92:227-35.
85. Meeprasert A, Hannongbua S, Kungwan N, Rungrotmongkol T. Effect of D168V mutation in NS3/4A HCV protease on susceptibilities of faldaprevir and danoprevir. *Molecular BioSystems.* 2016;12(12):3666-73.

86. Boonma T, Nutho B, Rungrotmongkol T, Nunthaboot N. Understanding of the drug resistance mechanism of hepatitis C virus NS3/4A to paritaprevir due to D168N/Y mutations: A molecular dynamics simulation perspective. *Computational biology and chemistry*. 2019;83:107154.
87. Maier JA, Martinez C, Kasavajhala K, Wickstrom L, Hauser KE, Simmerling C. ff14SB: Improving the Accuracy of Protein Side Chain and Backbone Parameters from ff99SB. *J Chem Theory Comput*. 2015;11(8):3696-713.
88. Ryckaert J-P, Ciccotti G, Berendsen HJC. Numerical Integration of the Cartesian Equations of Motion of a System with Constraints: Molecular Dynamics of n-Alkanes. *Journal of Computational Physics*. 1977;23:327.
89. Darden TA, York DM, Pedersen LG. Particle mesh Ewald: An $p\log(N)$ method for Ewald sums in large systems. *Journal of Chemical Physics*. 1993;98:10089-92.
90. Roe DR, Cheatham TE. PTRAJ and CPPTRAJ: Software for Processing and Analysis of Molecular Dynamics Trajectory Data. *J Chem Theory Comput*. 2013;9:7:3084-95.
91. Miller BR, McGee TD, Swails JM, Homeyer N, Gohlke H, Roitberg AE. MMPBSA.py: An Efficient Program for End-State Free Energy Calculations. *J Chem Theory Comput*. 2012;8(9):3314-21.
92. Shafagh M, Rahmani F, Delirez N. CuO nanoparticles induce cytotoxicity and apoptosis in human K562 cancer cell line via mitochondrial pathway, through reactive oxygen species and P53. *Iran J Basic Med Sci*. 2015;18(10):993-1000.

93. Kim YM, Bombeck CA, Billiar TR. Nitric oxide as a bifunctional regulator of apoptosis. *Circ Res.* 1999;84(3):253-6.
94. Lin KT, Xue JY, Lin MC, Spokas EG, Sun FF, Wong PY. Peroxynitrite induces apoptosis of HL-60 cells by activation of a caspase-3 family protease. *Am J Physiol.* 1998;274(4):C855-60.
95. Vousden KH, Prives C. Blinded by the Light: The Growing Complexity of p53. *Cell.* 2009;137(3):413-31.
96. Hollstein M, Sidransky D, Vogelstein B, Harris CC. p53 mutations in human cancers. *Science.* 1991;253(5015):49-53.
97. Hainaut P, Hollstein M. p53 and human cancer: the first ten thousand mutations. *Adv Cancer Res.* 2000;77:81-137.
98. Kao S-H, Wang W-L, Chen C-Y, Chang Y-L, Wu Y-Y, Wang Y-T, et al. Analysis of Protein Stability by the Cycloheximide Chase Assay. *Bio Protoc.* 2015;5(1):e1374.
99. Mengel A, Chaki M, Shekariesfahlan A, Lindermayr C. Effect of nitric oxide on gene transcription - S-nitrosylation of nuclear proteins. *Front Plant Sci.* 2013;4:293-.
100. Schonhoff CM, Daou MC, Jones SN, Schiffer CA, Ross AH. Nitric oxide-mediated inhibition of Hdm2-p53 binding. *Biochemistry.* 2002;41(46):13570-4.
101. Quader S, Kataoka K. Nanomaterial-Enabled Cancer Therapy. *Mol Ther.* 2017;25(7):1501-13.

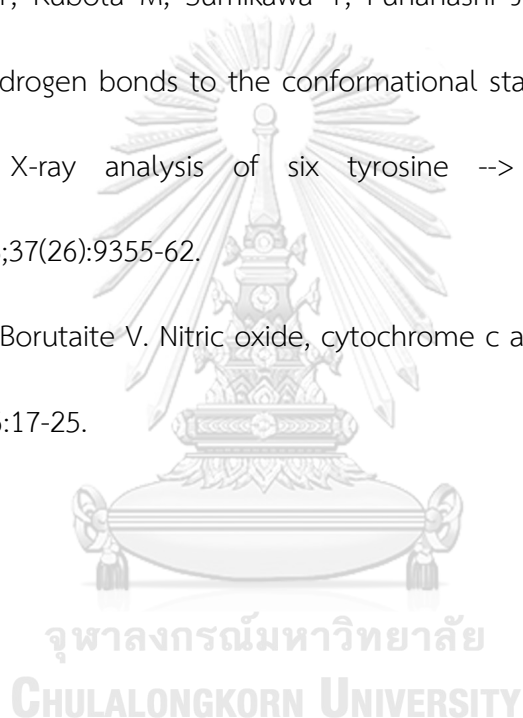
102. Patra JK, Das G, Fraceto LF, Campos EVR, Rodriguez-Torres MdP, Acosta-Torres LS, et al. Nano based drug delivery systems: recent developments and future prospects. *Journal of Nanobiotechnology*. 2018;16(1):71.
103. Boulaiz H, Alvarez PJ, Ramirez A, Marchal JA, Prados J, Rodríguez-Serrano F, et al. Nanomedicine: application areas and development prospects. *Int J Mol Sci*. 2011;12(5):3303-21.
104. Kulkarni M, Mazare A, Gongadze E, Perutkova Š, Kralj-Iglič V, Milošev I, et al. Titanium nanostructures for biomedical applications. *Nanotechnology*. 2015;26(6):062002.
105. Wu S, Weng Z, Liu X, Yeung KWK, Chu PK. Functionalized TiO₂ Based Nanomaterials for Biomedical Applications. *Advanced Functional Materials*. 2014;24(35):5464-81.
106. Kalaiarasi A, Sankar R, Anusha C, Saravanan K, Aarthy K, Karthic S, et al. Copper oxide nanoparticles induce anticancer activity in A549 lung cancer cells by inhibition of histone deacetylase. *Biotechnol Lett*. 2018;40(2):249-56.
107. Ma S, Miao H, Luo Y, Sun Y, Tian X, Wang F, et al. FePt/GO Nanosheets Suppress Proliferation, Enhance Radiosensitization and Induce Autophagy of Human Non-Small Cell Lung Cancer Cells. *Int J Biol Sci*. 2019;15(5):999-1009.
108. Satapathy SR, Mohapatra P, Preet R, Das D, Sarkar B, Choudhuri T, et al. Silver-based nanoparticles induce apoptosis in human colon cancer cells mediated through p53. *Nanomedicine*. 2013;8(8):1307-22.

109. Haupt S, Haupt Y. Importance of p53 for cancer onset and therapy. *Anticancer Drugs*. 2006;17(7):725-32.
110. Petpiroon N, Bhummaphan N, Soonnarong R, Chantarawong W, Maluangnont T, Pongrakhananon V, et al. Ti(0.8)O(2) Nanosheets Inhibit Lung Cancer Stem Cells by Inducing Production of Superoxide Anion. *Mol Pharmacol*. 2019;95(4):418-32.
111. Hsin YH, Chen CF, Huang S, Shih TS, Lai PS, Chueh PJ. The apoptotic effect of nanosilver is mediated by a ROS- and JNK-dependent mechanism involving the mitochondrial pathway in NIH3T3 cells. *Toxicol Lett*. 2008;179(3):130-9.
112. Loaiza-Pérez AI, Kenney S, Boswell J, Hollingshead M, Alley MC, Hose C, et al. Aryl hydrocarbon receptor activation of an antitumor aminoflavone: basis of selective toxicity for MCF-7 breast tumor cells. *Mol Cancer Ther*. 2004;3(6):715-25.
113. McLean L, Soto U, Agama K, Francis J, Jimenez R, Pommier Y, et al. Aminoflavone induces oxidative DNA damage and reactive oxidative species-mediated apoptosis in breast cancer cells. *Int J Cancer*. 2008;122(7):1665-74.
114. Tyagi A, Raina K, Gangar S, Kaur M, Agarwal R, Agarwal C. Differential effect of grape seed extract against human non-small-cell lung cancer cells: the role of reactive oxygen species and apoptosis induction. *Nutr Cancer*. 2013;65 Suppl 1(01):44-53.
115. Radi R. Oxygen radicals, nitric oxide, and peroxynitrite: Redox pathways in molecular medicine. *Proc Natl Acad Sci U S A*. 2018;115(23):5839-48.

116. Islam BU, Habib S, Ahmad P, Allarakha S, Moinuddin, Ali A. Pathophysiological Role of Peroxynitrite Induced DNA Damage in Human Diseases: A Special Focus on Poly(ADP-ribose) Polymerase (PARP). *Indian J Clin Biochem.* 2015;30(4):368-85.
117. Cobbs CS, Samanta M, Harkins LE, Gillespie GY, Merrick BA, MacMillan-Crow LA. Evidence for peroxynitrite-mediated modifications to p53 in human gliomas: possible functional consequences. *Arch Biochem Biophys.* 2001;394(2):167-72.
118. Batinić-Haberle I, Cuzzocrea S, Rebouças JS, Ferrer-Sueta G, Mazzon E, Di Paola R, et al. Pure MnTBAP selectively scavenges peroxynitrite over superoxide: comparison of pure and commercial MnTBAP samples to MnTE-2-PyP in two models of oxidative stress injury, an SOD-specific *Escherichia coli* model and carrageenan-induced pleurisy. *Free Radic Biol Med.* 2009;46(2):192-201.
119. Cuzzocrea S, Costantino G, Mazzon E, De Sarro A, Caputi AP. Beneficial effects of Mn(III)tetrakis (4-benzoic acid) porphyrin (MnTBAP), a superoxide dismutase mimetic, in zymosan-induced shock. *Br J Pharmacol.* 1999;128(6):1241-51.
120. Zhao Y, Yu H, Hu W. The regulation of MDM2 oncogene and its impact on human cancers. *Acta Biochim Biophys Sin (Shanghai).* 2014;46(3):180-9.
121. Chao C, Saito S, Kang J, Anderson CW, Appella E, Xu Y. p53 transcriptional activity is essential for p53-dependent apoptosis following DNA damage. *EMBO J.* 2000;19(18):4967-75.

122. Quesnel B, Preudhomme C, Oscier D, Lepelley P, Collyn-d'Hooghe M, Facon T, et al. Over-expression of the MDM2 gene is found in some cases of haematological malignancies. *Br J Haematol*. 1994;88(2):415-8.
123. Vassilev LT, Vu BT, Graves B, Carvajal D, Podlaski F, Filipovic Z, et al. In vivo activation of the p53 pathway by small-molecule antagonists of MDM2. *Science*. 2004;303(5659):844-8.
124. Sun J, Steenbergen C, Murphy E. S-nitrosylation: NO-related redox signaling to protect against oxidative stress. *Antioxidants & redox signaling*. 2006;8(9-10):1693-705.
125. Stamler JS, Hess DT. Nascent nitrosylases. *Nature Cell Biology*. 2010;12(11):1024-6.
126. Nakamura T, Tu S, Akhtar MW, Sunico CR, Okamoto S, Lipton SA. Aberrant protein s-nitrosylation in neurodegenerative diseases. *Neuron*. 2013;78(4):596-614.
127. Imamura K, Ogura T, Kishimoto A, Kaminishi M, Esumi H. Cell cycle regulation via p53 phosphorylation by a 5'-AMP activated protein kinase activator, 5-aminoimidazole-4-carboxamide-1-beta-D-ribofuranoside, in a human hepatocellular carcinoma cell line. *Biochem Biophys Res Commun*. 2001;287(2):562-7.
128. Levine AJ. p53, the cellular gatekeeper for growth and division. *Cell*. 1997;88(3):323-31.
129. Joerger AC, Fersht AR. Structure-function-rescue: the diverse nature of common p53 cancer mutants. *Oncogene*. 2007;26(15):2226-42.

130. Gencel-Augusto J, Lozano G. p53 tetramerization: at the center of the dominant-negative effect of mutant p53. *Genes Dev.* 2020;34(17-18):1128-46.
131. Takano K, Yamagata Y, Funahashi J, Hioki Y, Kuramitsu S, Yutani K. Contribution of Intra- and Intermolecular Hydrogen Bonds to the Conformational Stability of Human Lysozyme. *Biochemistry.* 1999;38(39):12698-708.
132. Yamagata Y, Kubota M, Sumikawa Y, Funahashi J, Takano K, Fujii S, et al. Contribution of hydrogen bonds to the conformational stability of human lysozyme: calorimetry and X-ray analysis of six tyrosine --> phenylalanine mutants. *Biochemistry.* 1998;37(26):9355-62.
133. Brown GC, Borutaite V. Nitric oxide, cytochrome c and mitochondria. *Biochem Soc Symp.* 1999;66:17-25.



VITA

NAME Rapeepun Soonnarong

DATE OF BIRTH 17 January 1990

PLACE OF BIRTH Roi-Et, Thailand

INSTITUTIONS ATTENDED Master of Science in Medical Biochemistry, Chulalongkorn University
Bachelor of Science in Biochemistry, Chulalongkorn University

HOME ADDRESS 45/5 Bang Kruai-Sainoi Rd. Bang Si Thong, Bang Kruai, Nonthaburi, 11130

PUBLICATION

1. N. Petpiroon, N. Bhummaphan, R. Soonnarong, W.Chantarawong, T.Maluangnont, V. Pongrakhananon, P. Chanvorachote. (2019). TiO₂ Nanosheets Inhibit Lung Cancer Stem Cells by Inducing Production of Superoxide Anion. *Molecular Pharmacology*, 95 (4), 418-432.
2. R. Soonnarong, S. Tungsukruthai, B. Nutho, T. Rungrotmongkol, C. Vinayanuwattikun, T.Maluangnont, P. Chanvorachote. (2021). Titania nanosheet generates peroxy nitrite-dependent S-nitrosylation and enhances p53 function in lung cancer cells. *Pharmaceutics*, 13(8): 1233.
3. R. Soonnarong, I. Dwi Putra, N. Sriratanasak, B. Sritularak, P. Chanvorachote. (2022). Artonin F Induces the Ubiquitin-Proteasomal Degradation of c-Met and Decreases Akt-mTOR Signaling. *Pharmaceutics*, (15)5; 663.